COMPARISON AND CONVERGENCE STUDIES OF NONLINEAR FINITE ELEMENT BEAM-COLUMN MODELS

by

George Michael Brown

Thesis submitted to the Graduate Faculty of the
Virginia Polytechnic Institute and State University
in partial fulfillment of the requirements for the degree of
MASTER OF SCIENCE
in
Civil Engineering

APPROVED:

S. M. Holzer, Chairman

R. H. Plaut

A. E. Somers

May, 1977

Blacksburg, Virginia

ACKNOWLEDGMENTS

My deep appreciation is extended to Dr. Siegfried M. Holzer for his many suggestions and support and his editing this report. Special thanks are given to Dr. R. H. Plaut who was invaluable in editing this report. I wish to express my gratitude to Dr. A. E. Somers for the suggestions he offered in the course of this study. The efforts of and are gratefully acknowledged. Thanks to for the preparation of the figures herein and for typing the report.

LM/MRJ 6/6/77

TABLE OF CONTENTS

LIST OF FIGURES

LIST OF TABLES

CHAPTER I

INTRODUCTION

This investigation consists of comparison and convergence studies of two finite element beam-column displacement models. These models are geometrically nonlinear and have elastic and inelastic material modeling capabilities.

The original element model and system model, as well as the computer code framework used herein, were developed by Holzer, et al. [1]. Bradshaw conducted tests on the model [2]. The computer code was modified for inelastic behavior by Shiflett [12], who subsequently tested the model's inelastic response predictions. This element model, which will be referred to in this investigation as model 1, was the first element model of the computer code SINGER [1].

Modifications to SINGER were performed and documented in a technical report by Holzer, et al. [4]. These modifications resulted in a different but related element model, which will be designated as model 2 for comparison purposes. This is the current element model being used in SINGER.

A modification of model 2 is made in this study, resulting in model 3.

Four test problems are considered to evaluate the models' quality of response predictions. The models are tested over the entire range of response, from the linearly elastic and geometrically linear range to the inelastic geometrically nonlinear

range. In every test problem, only static conservative loading is applied.

Models 2 and 3 form the basis of this investigation and will be examined in all test problems. Model 1 will be used for comparison in one test problem to exhibit the rationale for certain features of models 2 and 3.

The classical continuum beam-column model will be used as a basis for convergence studies. Macro and micro response parameters of the models will be examined. The models' relative computational efficiencies will also be compared.

CHAPTER II

MODEL DESCRIPTIONS

The system model and solution process used in this investigation are identical for element models 1, 2, and 3.

System Model

The system model is an assemblage of one-dimensional finite element beam-column models rigidly connected at external nodes, capable of representing two-dimensional skeletal structures. Actions on the system are represented by generalized forces applied at the external (joint) nodes. A global reference system is used to describe the initial and displaced configuration of the assemblage. Geometric nonlinearities are modeled by formulating equilibrium for the deformed state and a nonlinear strain-displacement relation.

The state of the system is completely defined by an energy function which is a scalar function of the generalized coordinates and forces of the system. The energy function is defined as

$$E = \Pi + \Omega \tag{1}$$

$$\Pi = \sum_{m=1}^{NM} \Pi_m \tag{2}$$

$$\Omega = -Q^T q = -\sum_{j=1}^{n} Q_i q_i \tag{3}$$

where

NM = number of elements

Π_m = internal energy of m^{th} element

Q_i = i^{th} generalized force component

q_i = i^{th} generalized coordinate

n = number of generalized coordinates

The equilibrium path of the system is established at discrete load levels. The state of the system in the linear range is defined by the nodal displacements. In the nonlinear range, the generalized coordinates are related to the equilibrium path to define the system state.

The discrete equilibrium states are obtained by minimizing the energy function. Application of the stationarity condition to Equation 1 yields the equations of equilibrium [14]

$$G_i \equiv \frac{\partial \Pi}{\partial q_i} - Q_i = 0 \qquad i = 1, 2, \ldots, n \qquad (4)$$

These equations are nonlinear functions of the generalized coordinates, and they define the energy function gradients, G_i, used in the solution process.

Solution Process

The solution process initiates at a known equilibrium state. The actions are incremented and the energy function minimized to yield a "new" stable equilibrium configuration.

The minimization procedure used in this work is the variable-metric gradient algorithm originally developed by Davidon and modified by Fletcher and Powell [17].

At each load step, the energy function is minimized by conducting a series of one-dimensional searches. These searches begin at X_1, the vector of generalized coordinates of the previous equilibrium state. The searches proceed according to the formula [16]

$$X_{i+1} = X_i + \alpha_i P_i \tag{5}$$

where

i = i^{th} search

and

X_i = i^{th} trial solution

P_i = i^{th} directional search vector

α_i = some positive constant

Each α_i is determined by minimizing the energy function along P_i. The P_i's are functions of the left side of Equation 4, the system gradients. P_{i+1} is a function of the gradients evaluated at X_{i+1} and X_i. For inelastic analysis, the gradients and energy function must be evaluated numerically. (Gaussian guadrature is employed for this purpose).

Convergence of the solution process is obtained when $(P_i^T P_i)^{1/2}$ and the individual components of P_i are less than a prescribed value. The value used in this study is 10^{-7}.

This minimization procedure guarantees quadratic convergence. It will minimize a quadratic function of n variables in at most n iterations. No general statement can be made, however, for

higher ordered functions such as the energy function used in this investigation. The amount of computation required to establish a "new" equilibrium configuration depends on the sensitivity of the energy function to changes in the generalized coordinates [16].

Element Models

Discretization of a continuum model is accomplished by subdividing the model into discrete finite elements. The element models are one-dimensional beam-column models whose axial and flexural deformations are geometrically coupled. Inelastic behavior is represented by the element's constitutive relation.

The element models being studied are line elements that conform to the classical beam-column assumptions [4]. These assumptions are:

1. Normal strains and rotations are infinitesimal (their squares are negligible as compared to unity).
2. Plane sections remain plane and normal to the deformed reference axis.
3. The plane of bending corresponds to the longitudinal plane of symmetry.
4. Shear deformations are negligible.
5. The material behavior at any point in the member is described by the constitutive law.

As in the classical model, the state of any point in the finite element can be described relative to the displaced reference axis. Although strains and rotations are required to be small on an

element basis, no restrictions are placed on deformations of the assemblage if appropriate sub-division of the continuum is employed.

The state of an element is completely defined by its internal energy which is a function of the element's deformation vector. This vector is a function of the element's generalized coordinates with all rigid body modes eliminated.

Model Differences

Models 1, 2, and 3 differ in the following manner: The local reference frame of model 1 is different from the local reference frame of models 2 and 3. The strain field of each model is different.

Frame of Reference

The local deformation frame of reference moves in accordance with the rigid body motions of the element. For model 1, the local frame of reference is rigidly attached to the joint at the origin of the element (see Figure 1a). This reference frame exhibited a directional tendency which magnified roundoff and discretization errors. For a description and analysis of this tendency, see Ref. 4.

Models 2 and 3 employ the symmetric reference system developed by Holzer, et al. [4]. This reference system reflects the inherent symmetry of the element models (see Figures 1b and c).

Strain Field

The strain field and internal energy of an element are functions of the corresponding element deformation vector, $\bar{u}$. The element

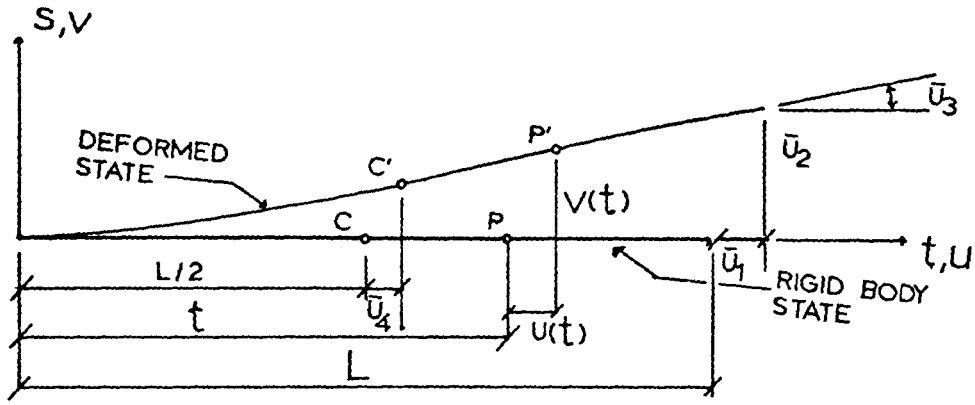

a. Model 1 $X = tL$, $Y = sL$

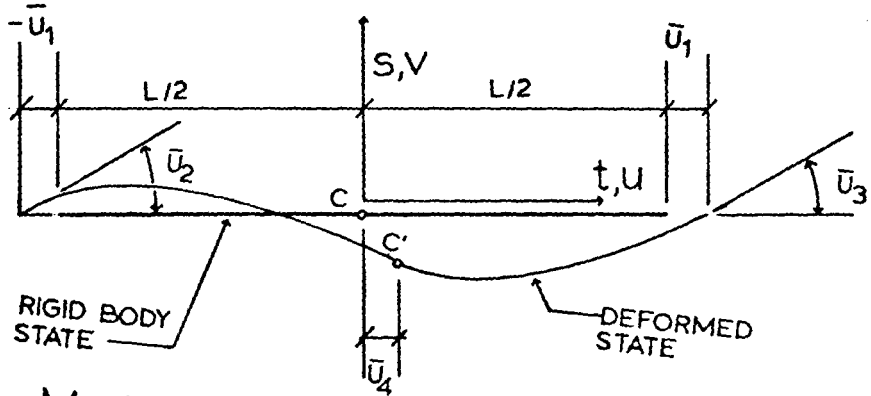

b. Model 2 $X = L/2(t+1)$, $Y = sL$

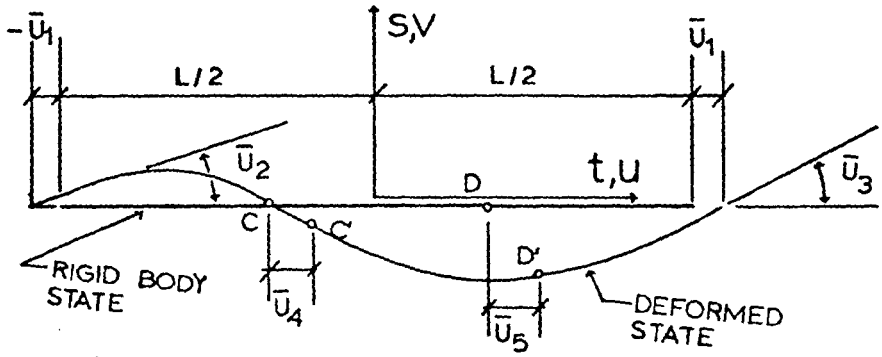

c. Model 3 $X = L/2(t+1)$, $Y = sL$

FIG. 1 ELEMENT MODEL DESCRIPTIONS

deformation vector describes the element displacements and rotations relative to the local moving frame of reference. This vector is a function of the generalized coordinates of the element. The transformations relating the deformation vector and generalized coordinates for model 1 are found in Ref. 1. The transformations for models 2 and 3 are identical and can be found in Ref. 4. This is because $\bar{u}_1$, $\bar{u}_2$, and $\bar{u}_3$ (see Figures 1b and c) are defined identically in terms of the joint generalized coordinates for both models. The models differ in the internal deformation components, which are generalized coordinates requiring no transformations.

The internal deformation components for the element models being considered correspond to axial degrees of freedom in the interior of the elements. Lagrangian interpolation is employed in describing each element's axial displacement field in terms of the element's axial deformation components. Therefore, introduction of n internal deformation components increases the order of the element's axial polynomial displacement function by n in x, the element longitudinal coordinate.

The shape function corresponding to an internal axial deformation component assumes zero values identically on the boundaries of the element. The same shape function assumes unity at the longitudinal coordinate location of the deformation component in the interior of the element. This shape function is occasionally referred to as an "internal mode" [6].

Models 1 and 2 have one internal deformation component each; hence, the respective element axial displacement functions are complete second-order polynomials in x. Model 3 has two internal deformation components resulting in a complete third-order polynomial representation in x of the element axial displacement function.

Models 1, 2, and 3 conform to the first-order nonlinear strain-displacement relation

$$\varepsilon(x,y) = \frac{du}{dx} + \frac{1}{2}\left(\frac{dv}{dx}\right)^2 - y\frac{d^2v}{dx^2} \tag{6}$$

where u, v, x, and y are defined as in Figure 1 and $\varepsilon(x,y)$ is the normal strain at the point (x,y). The strain can be resolved into two components: $\varepsilon_a(x,0)$, the extensional normal strain along the reference axis and $\varepsilon_b(x,y)$, the normal elementary bending strain.

The extensional strain along the reference axis is defined as

$$\varepsilon_a(x,0) = \frac{du}{dx} + \frac{1}{2}\left(\frac{dv}{dx}\right)^2 \tag{7}$$

The first term of Equation 7 describes the normal strain produced by axial deformation of the reference axis. The second term represents the first-order nonlinear extensional strain contribution associated with the coupling of flexural and axial deformations.

The elementary normal bending strain is defined by the relation

$$\varepsilon_b(x,y) = -y\left(\frac{d^2v}{dx^2}\right) \tag{8}$$

For the finite element models, the discretized normal strain representing Equation 6, $\bar{\varepsilon}(x,y)$, can be resolved into the components, $\bar{\varepsilon}_a(x,0)$ and $\bar{\varepsilon}_b(x,y)$ which represent Equations 7 and 8 of the continuum model, respectively.

The discretized normal elementary bending strain, $\bar{\varepsilon}_b(x,y)$, is a complete first-order polynomial in x and y for models 1, 2, and 3.

For model 1, the axial deformation contribution to the extensional strain is a first-order polynomial in x, while the coupling term is represented by a fourth-order polynomial in x. This implies that the strain cannot vanish identically along the reference axis, i.e. the model cannot predict exact bending strains for a simple bending state.

The extensional normal strain along the reference axis is defined for model 2 in terms of the normalized longitudinal coordinate t as

$$\bar{\varepsilon}_a(t,0) = \frac{2}{L}\bar{u}_1 + \frac{1}{15}(\bar{u}_2^2 - \frac{1}{2}\bar{u}_2\bar{u}_3 + \bar{u}_3^2) + [\frac{1}{16}(\bar{u}_3^2 - \bar{u}_2^2) - \frac{4}{L}\bar{u}_4]\, t \tag{9}$$

where t, L, $\bar{u}_1$, $\bar{u}_2$, $\bar{u}_3$, and $\bar{u}_4$ are as defined in Figure 1b.

The contributions of the axial deformation components $\bar{u}_1$ and $\bar{u}_4$ to Equation 9 represent the extensional normal strain produced by axial deformation. The contributions of $\bar{u}_2$ and $\bar{u}_3$ to Equation 9

represent the coupling of axial and flexural deformations. This strain contribution has been constrained to be a linear function in t like the strain component produced by axial deformation. This permits the extensional normal strain to be identically zero along the reference axis. For a derivation of the strain field of model 2, see Ref. 4.

The extensional normal strain along the reference axis is defined for model 3 as

$$\bar{\varepsilon}_a(t,0) = \frac{27}{8L}\left(\frac{-2}{27}\bar{u}_1 - \bar{u}_4 + \bar{u}_5\right) + \frac{1}{40}\left(\bar{u}_2 + \bar{u}_3\right)^2$$

$$- \frac{9}{4}\left[\frac{1}{L}\left(\bar{u}_5 + \bar{u}_4\right) + \frac{1}{27}\left(u_2^2 - \bar{u}_3^2\right)\right]t \qquad (10)$$

$$+ \frac{81}{8}\left[\frac{1}{L}\left(\frac{2}{3}\bar{u}_1 + \bar{u}_4 - \bar{u}_5\right) + \frac{1}{81}\left(\bar{u}_2 - \bar{u}_3\right)^2\right]t^2$$

where t, L, $\bar{u}_1$, $\bar{u}_2$, $\bar{u}_3$, $\bar{u}_4$ and $\bar{u}_5$ are as defined in Figure 1c.

The extensional normal strain produced by axial deformation is represented by the contributions of $\bar{u}_1$, $\bar{u}_4$ and $\bar{u}_5$, the models axial deformation components, to Equation 10. The contribution of the coupling of axial and flexural deformations to the extensional normal strain is represented by $\bar{u}_2$ and $\bar{u}_3$ in Equation 10. The coupling term has been constrained to be quadratic in t. Since the normal strain caused by axial deformation is quadratic in t also, this permits the extensional normal strain to vanish identically along the reference axis, as in model 2. For a derivation of the strain-field corresponding to model 3, see the Appendix.

If the rate of convergence of a finite element is determined by the ability of its strain function to represent arbitrary polynomial shapes as stated by Fried [18], model 3 should theoretically perform as well or better than model 2 in convergence studies. Zienkiewicz states "as a general rule that as the order of an element increases so the total number of unknowns in a problem can be reduced for a given accuracy of representation" [5]. It should be noted that although model 3 has a higher order polynomial description of the element axial displacement field than model 2, both models have identical polynomial descriptions of the element transverse displacement field.

In the next chapter, four test problems are examined to determine the differences and similarities of the response predictions of the two models.

CHAPTER III

TEST PROBLEMS

Four test problems are examined in this chapter using models 2 and 3. The purposes for examining these problems are:

1. To compare the accuracy of response predictions of the two models for a given mesh of elements.
2. To compare convergence of the response predictions for both models as the mesh is refined.
3. To compare the relative computational efficiencies of the models.

Model 1 will be used for comparison in the first test problem. Various measures of the accuracy of response predictions will be used in each test.

Response Measures

The accuracy of response predictions of the models is governed by their energy representations. Two types of errors occur in these representations; they are the discretization and quadrature errors [4]. (Another source of error that results from the finite element method but is not directly associated with the energy representations of the models is round-off error: the error produced by numerical manipulations in the computer [15]. This error will not be considered in this study.)

The quadrature error is produced by numerical integration of the internal-energy density over the volume of the finite element [4].

Variable Gaussian quadrature is employed in the computer code used in this study. In the elastic range, quadratures have been selected to integrate the internal-energy densities over the volumes of the finite elements exactly [4]. In the inelastic range, the Gauss point distributions have been selected to eliminate the influences of quadrature error on the accuracy of the response predictions.

The discretization error is produced by representing a continuum model by a finite number of generalized coordinates. In order to control this error, refinements in the finite element approximation should yield a solution that converges to the exact solution of the corresponding continuum model [20]. If a finite element model satisfies the conditions of completeness and conformity, successive refined approximations will yield convergence of potential energy to that of the corresponding continuum model in the linear elastic domain [20]. If these conitions are satisfied, the finite element method becomes a special case of the Ritz method, which guarantees convergence to the exact solution in the mean-square sense [7,19].

Models 1, 2, and 3 satisfy the conditions of completeness and conformity; therefore, any mesh refinement in the linear elastic range of response will result in monotonic convergence of the discretized potential energy to that of the corresponding continuum model. No general statement can be made, a priori, regarding pointwise behavior of the elements under consideration [5]. Convergence cannot be

guaranteed for the nonlinear range of response in any sense [5]. Numerical tests are necessary to evaluate the response characteristics of the models in the nonlinear range of response.

Macro and micro model response predictions at discrete points within the assemblages of finite elements are investigated for the test problems considered in this chapter. In the first three test problems, the accuracy of the response predictions is evaluated relative to the classical beam and beam-column models. The fourth test problem consists of a comparison with an existing finite element solution.

For each test problem, the average solution times and minimization efforts per load increment required to define the equilibrium paths predicted by models 2 and 3 are examined. This information gives an indication of the relative computational efficiencies of the models. Computational efficiency is affected by parameters such as mesh sizes, quadrature rules, and load increments. These parameters have been made equivalent for the models in all cases to provide meaningful efficiency comparisons. It should be noted that these efficiency comparisons are valid only for the minimization process[1] employed in this study.

The results of the test problems follow. An interpretation and evaluation of the results will be given in Chapter IV.

---

[1] The minimization process used in this study is the Davidon Fletcher Powell computer routine obtained from the computer library at the Computing Center of Virginia Polytechnic Institute and State University, Blacksburg, Virginia.

Single Element Test

The purpose of this test is to compare the elastic and inelastic micro response predictions of models 1, 2, and 3. The models are subjected to a simple bending state.

The test consists of a single element cantilever beam with a concentrated moment applied at the free end. The problem is defined in Figure 2. L/r ratios of 13, 52, and 208 are used for each model. An eight by four Gauss rule is employed to eliminate the influence of quadrature errors.

The accuracy of the micro response predictions of each model is measured by the variance of the approximate extreme fiber compressive strain value at the fixed end of the element with the exact value obtained from an analytical solution. The error is given by

$$e_m = \left| \frac{\bar{\varepsilon}_c - \varepsilon_c}{\varepsilon_c} \right| \times 100 \qquad (9)$$

where e_m is the percent micro response error, $\bar{\varepsilon}_c$ is the approximate strain value and ε_c is the exact strain value [4].

In Tables 1 and 2, the elastic micro response error is tabulated for moments of 6 and 36 kip inches, respectively. The approximate bending and extensional strain contributions correspond to $\bar{\varepsilon}_c^b$ and $\bar{\varepsilon}_c^a$, respectively. The error produced by model 1 approaches zero as the mesh is refined (as L/r decreases). The error in the values predicted by model 1 is due primarily to the extensional

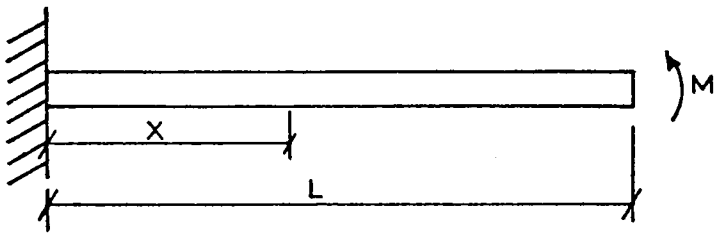

a. Longitudinal Section

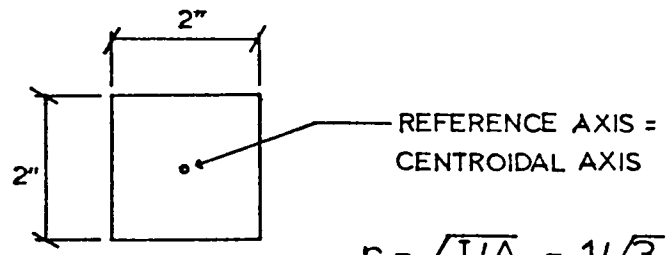

b. Cross Section

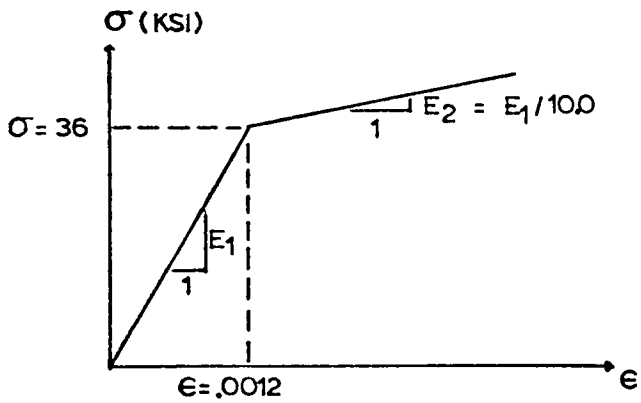

c. Constitutive Law

FIG. 2 SINGLE ELEMENT TEST DESCRIPTION

TABLE 1. ELASTIC MICRO RESPONSE ERROR - SINGLE ELEMENT TEST, M = 6 kip inches

Model	L/r	Exact $\epsilon_c(10^3)$	$\bar{\epsilon}_c(10^3)$	$\bar{\epsilon}_c^{\,b}(10^3)$	$\bar{\epsilon}_c^{\,a}(10^3)$	$e_m(\%)$
1	208	-0.150	-0.128	-0.153	0.025	14.7
2	208	-0.150	-0.150	-0.150	0.000	0.0
3	208	-0.150	-0.150	-0.150	0.000	0.0
1	52	-0.150	-0.148	-0.150	0.002	1.3
2	52	-0.150	-0.150	-0.150	0.000	0.0
3	52	-0.150	-0.150	-0.150	0.000	0.0
1	13	-0.150	-0.150	-0.150	0.000	0.0
2	13	-0.150	-0.150	-0.150	0.000	0.0
3	13	-0.150	-0.150	-0.150	0.000	0.0

TABLE 2. ELASTIC MICRO RESPONSE ERROR - SINGLE ELEMENT TEST, M = 36 kip inches

Model	L/r	$\varepsilon_c(10^3)$	$\bar{\varepsilon}_c(10^3)$	$\bar{\varepsilon}_c^{\,b}(10^3)$	$\bar{\varepsilon}_c^{\,a}(10^3)$	$e_m(\%)$
1	208	-0.900	-0.620	-1.060	0.440	31.1
2	208	-0.900	-0.900	-0.900	0.000	0.0
3	208	-0.900	-0.900	-0.900	0.000	0.0
1	52	-0.900	-0.843	-0.903	0.060	6.3
2	52	-0.900	-0.900	-0.900	0.000	0.0
3	52	-0.900	-0.900	-0.900	0.000	0.0
1	13	-0.900	-0.896	-0.900	0.004	0.4
2	13	-0.900	-0.900	-0.900	0.000	0.0
3	13	-0.900	-0.900	-0.900	0.000	0.0

strain contribution which should be zero identically along the element for a simple bending state.

As shown in Tables 1 and 2, models 2 and 3 give exact strain values in the elastic range. The corresponding linearly elastic continuum beam solution predicts a linear strain variation through the depth of the cross-section and constant strain at any given fiber along the length of the beam (the extensional strain is zero at every point in the beam). Models 2 and 3 can represent this strain state because the extensional strain is allowed to vanish, as discussed in Chapter II. The bending strain functions of both models are identical and are first-order polynomials in the longitudinal and transverse coordinates of an element. Hence, an exact representation of this continuum strain state is possible.

The component distributions of the extreme fiber compressive strain predicted by models 2 and 3 are presented in Table 3. The component values are shown at various points along the length of the beam when M = 36 kip inches and L/r = 208. The strain component caused by axial deformation is $\frac{d\bar{u}}{dx}$. The extensional strain produced by the coupling of axial and flexural deformations is represented by $\frac{1}{2}(\frac{d\bar{v}}{dx})^2$. Observe that each extensional strain component of model 2 is not equal to the corresponding component predicted by model 3. This is because the models have different polynomial representations of these components. The sum of the components, the extensional strain $\bar{\varepsilon}_a^c$, is identically zero for both models along the length of the beam. This is as predicted by the continuum model.

TABLE 3. STRAIN[1] COMPONENT DISTRIBUTIONS - SINGLE ELEMENT TEST

M = 36 kip inches

	Model 2				Model 3			
$\frac{x}{L}$	$\frac{d\bar{u}}{dx}$	$\frac{1}{2}(\frac{dv}{dx})^2$	$\bar{\varepsilon}_a^c$	$\bar{\varepsilon}_b^c$	$\frac{d\bar{u}}{dx}$	$\frac{1}{2}(\frac{dv}{dx})^2$	$\bar{\varepsilon}_a^c$	$\bar{\varepsilon}_b^c$
0.000	-0.486	0.486	0.0	-0.900	-1.460	1.460	0.0	-0.900
0.125	-0.486	0.486	0.0	-0.900	-0.820	0.820	0.0	-0.900
0.250	-0.486	0.486	0.0	-0.900	-0.365	0.365	0.0	-0.900
0.375	-0.486	0.486	0.0	-0.900	-0.091	0.091	0.0	-0.900
0.500	-0.486	0.486	0.0	-0.900	-0.000	0.000	0.0	-0.900
0.625	-0.486	0.486	0.0	-0.900	-0.091	0.091	0.0	-0.900
0.750	-0.486	0.486	0.0	-0.900	-0.365	0.365	0.0	-0.900
0.875	-0.486	0.486	0.0	-0.900	-0.820	0.820	0.0	-0.900
1.000	-0.486	0.486	0.0	-0.900	-1.460	1.46	0.0	-0.900

[1]All Strains x 10^3

The inelastic micro response error is shown graphically in Figure 3. The micro response error produced by model 1 does not approach zero as the mesh is refined in the inelastic range.

The micro response errors of models 2 and 3 are identical in the inelastic range. The error is unaffected by decreasing the element length. This is true for two reasons: 1. the extensional strain vanishes throughout each element and 2. the constant bending strain state is not a function of the element's length. Therefore, mesh refinement will yield no changes in the accuracy of the micro response prediction of models 2 and 3.

Considering the entire inelastic range, models 2 and 3 predict consistantly more accurate micro responses than model 1.

The relative computational efficiencies of models 2 and 3 are shown in Table 4. Model 2 is seen to be more efficient in every case than model 3 in this test for an identical level of accuracy of response predictions. Observe that as the L/r ratio of model 3 is reduced, the average number of minimizations per load increment increases.

Elastica Problem

This problem is investigated to compare the linearly elastic, geometrically nonlinear response predictions of the models. The elastica problem deals with the determination of buckled forms of elastic columns [7].

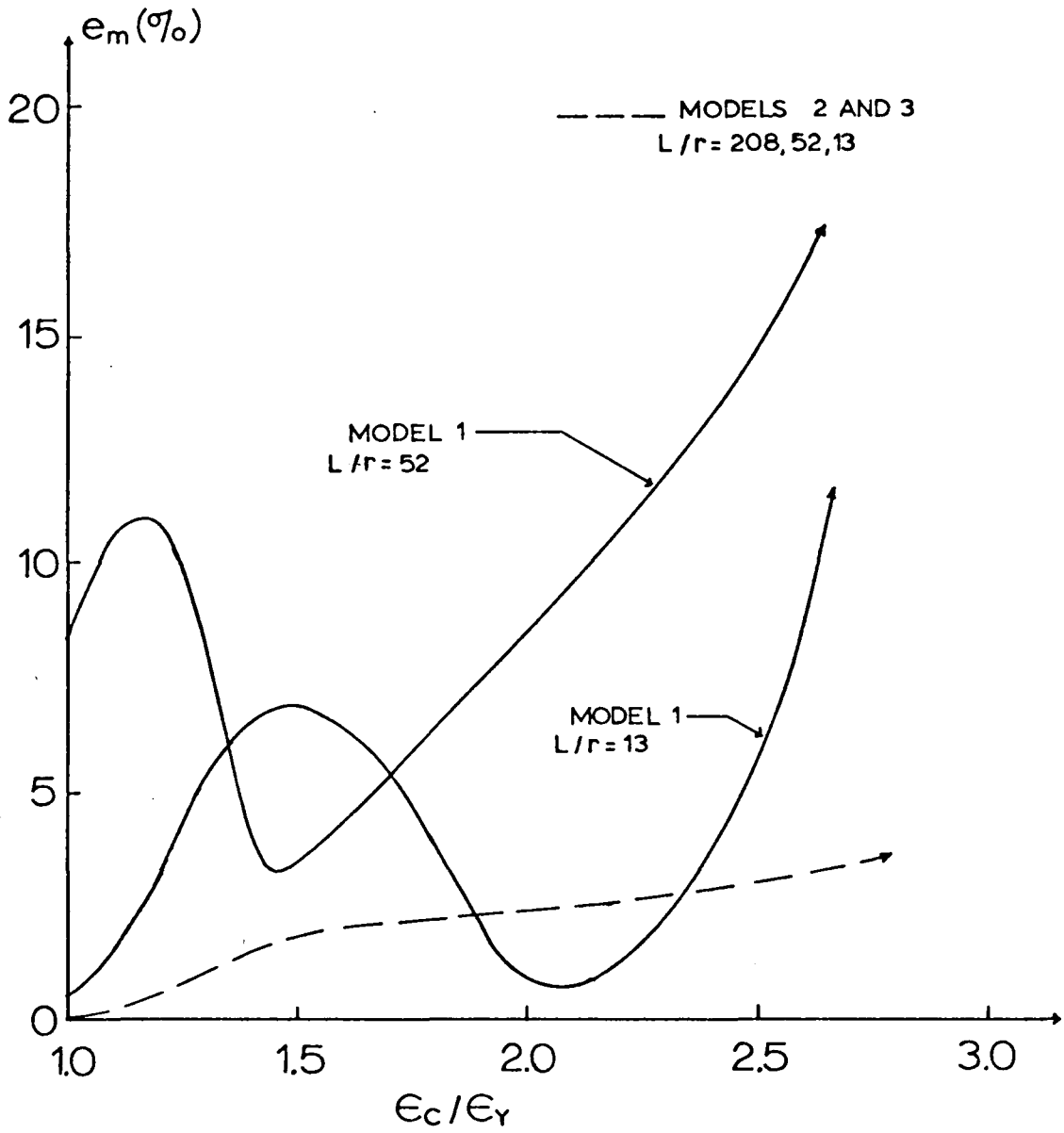

FIG. 3 INELASTIC MICRO RESPONSE ERROR– SINGLE ELEMENT TEST

TABLE 4. RELATIVE COMPUTATIONAL EFFICIENCIES - SINGLE ELEMENT TEST

Model	L/r	Avg. No. of Mins. Per Load Increment[1]	Avg. Solution Time Per Load Increment[2]
2	208	13.6	9.6
3	208	14.1	14.1
2	52	12.0	7.4
3	52	16.5	12.4
2	13	12.8	7.6
3	13	21.2	12.9

[1]Load increment is 2 in. kips

[2]Seconds

The elastica problem was originally investigated by Euler. The basis of this comparison is the continuum solution presented by Timoshenko and Gere for a cantilever column [3]. This solution is established on the formulation of the exact expression for the curvature of the buckled column, and hence, the "exact" differential equation of the column. (The solution disregards axial shortening of the column due to compression [3]). The displacements and rotation of the free end of the column are given by elliptic integrals.

The finite element analysis is conducted with four and eight element meshes using models 2 and 3. (For the results of a similar analysis conducted with model 1 see Ref. 2). The cross-section is a two inch square. The centroidal axis is coincidental with the reference axis; i.e. no eccentricity is applied in loading. Linear elasticity is assumed throughout the loading range. The problem is defined in Figure 4. (P_E corresponds to the Euler buckling load.)

For this problem, the element strain energies have been obtained in closed-form for models 2 and 3. Since linearly elastic material response is assumed, the models' respective strain-energy density expressions can be obtained in closed-form. The strain-energy density expressions of each model can be integrated explicitly over the volumes of the corresponding elements. This yields an element's strain energy contribution to the strain energy of the system. The element gradient contributions to the system gradients

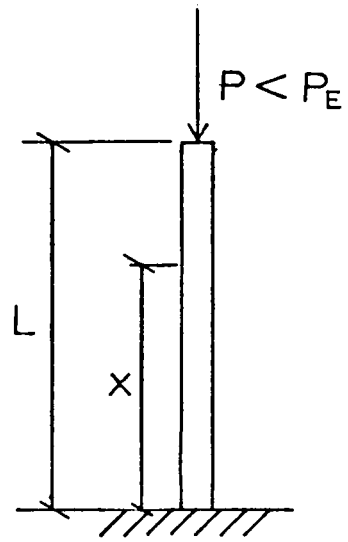

a. Unbuckled State

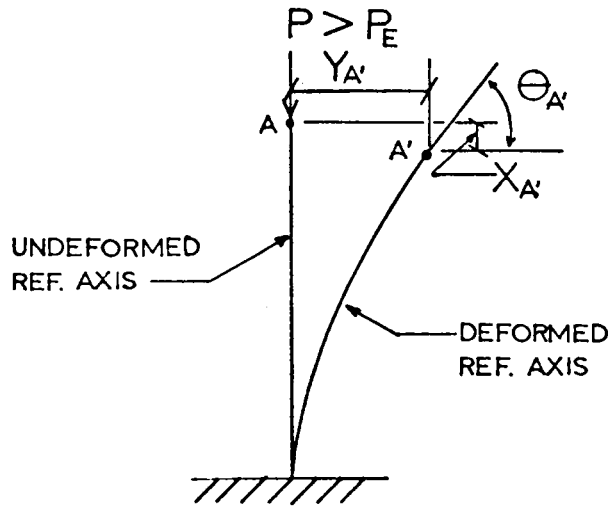

b. Post-Buckled State

FIG. 4 ELASTICA PROBLEM DESCRIPTION

can be obtained for both models in closed form from the respective element strain energies. This increases the computational efficiencies of both models as compared to corresponding solutions obtained using numerical integration to determine the strain energies of the models.

The post-buckling equilibrium paths predicted by the models are obtained for an axial load range of approximately 100 to 190% of the Euler load. The energy functions of both models are extremely sensitive to variations of the generalized coordinates in the proximity of the Euler load (approximately 1.0 to 1.1 x P_E). Therefore, small load increments in the axial load must be used in this vicinity of the Euler load. As the energy functions become less sensitive, greater load increments can be used.

Large displacements and rotations are characteristic of post-buckling analyses. Therefore, subdivision of the column into an assemblage of elements is required to insure adherence to the assumption stated in Chapter II of infinitesimal element strains and rotations. This permits large nodal displacements and rotations of the assemblages of both models.

The macro response predictions of both models are identical at every load level. These predictions include the system energies, displacements and rotations. The transverse tip displacement for the eight element meshes as compared to the corresponding elliptic integral solution is shown in Figure 5.

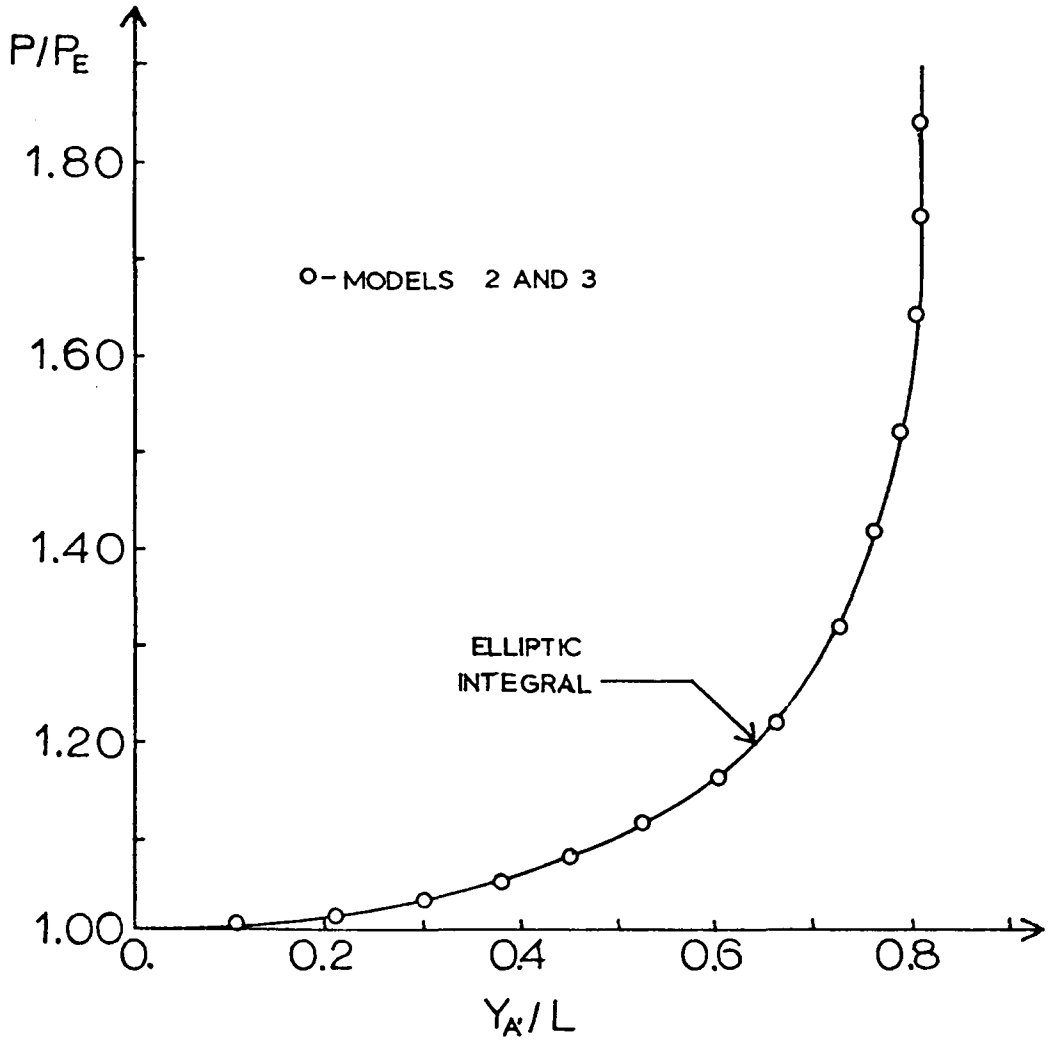

FIG. 5 ELASTICA PROBLEM
TRANSVERSE TIP DISPLACEMENT
8 ELEMENT MESH

The measure of micro response error used in this test is identical to that used in the single element test (see Equation 9). (The "exact" strain value can be computed at the fixed end of the column using the transverse tip displacement predicted by the corresponding elliptic integral to calculate the stress resultants.) The micro response error, e_m, is identical for models 2 and 3 at all load levels.

The total strain values are identical for both models at every point in the assemblages. The individual components of the extensional strain values predicted by model 2 are not equal to the corresponding components predicted by model 3. However, the extensional strain values are identical for both models and are constant throughout the length of an element. The component distributions of the extreme fiber compressive strain values predicted by each model are shown in Table 5 for various points along the element at the fixed end of the four element mesh when $P = 1.518 \times P_E$.

Since the material behavior in this test is linearly elastic, the energy function corresponds to the potential energy of the system, V. In Table 6, the potential energy, the errors in the transverse and axial displacements as compared to the corresponding elliptic integral solutions, and the micro response error are presented. These response predictions are tabulated for the four and eight element meshes at increasing load levels. All values are identical for models 2 and 3.

TABLE 5. COMPONENT STRAIN DISTRIBUTION ALONG ELEMENT AT FIXED END OF 4 ELEMENT MESH[1] - ELASTICA PROBLEM, $P = 1.518 \times P_E$

	Model 2				Model 3			
$\frac{x}{L}$	$\frac{d\bar{u}}{dx}$	$\frac{1}{2}(\frac{d\bar{v}}{dx})^2$	$\bar{\varepsilon}_c{}^a$	$\bar{\varepsilon}_c{}^b$	$\frac{d\bar{u}}{dx}$	$\frac{1}{2}(\frac{d\bar{v}}{dx})^2$	$\bar{\varepsilon}_c{}^a$	$\bar{\varepsilon}_c{}^b$
0.000	-21.852	21.816	-0.036	-16.761	-64.463	64.427	-0.036	-16.761
0.031	-21.700	21.664	-0.036	-16.534	-36.430	36.394	-0.036	-16.534
0.062	-21.548	21.512	-0.036	-16.307	-16.349	16.313	-0.036	-16.307
0.094	-21.397	21.361	-0.036	-16.080	-4.2190	4.183	-0.036	-16.080
0.125	-21.245	21.209	-0.036	-15.853	-0.0407	0.005	-0.036	-15.853
0.156	-21.093	21.057	-0.036	-15.626	-3.8139	3.778	-0.036	-15.626
0.187	-20.941	20.905	-0.036	-15.398	-15.539	15.503	-0.036	-15.398
0.218	-20.789	20.753	-0.036	-15.171	-35.215	35.179	-0.036	-15.171
0.250	-20.637	20.601	-0.036	-14.944	-62.842	62.805	-0.036	-14.944

[1] All Values x 10^3

TABLE 6. MACRO AND MICRO RESPONSE PREDICTIONS[1]

ELASTICA PROBLEM

P/P_E	N	V $\times 10^{-4}$ (lb-in)	% Displacement error[2]		e_m(%)
			X_A'	Y_A'	
1.015	4	-0.013	1.93	1.68	0.43
	8	-0.013	1.72	1.59	1.15
1.063	4	-0.028	1.20	0.43	0.90
	8	-0.029	1.16	0.41	0.07
1.152	4	-1.138	0.13	0.27	1.52
	8	-1.139	0.15	0.28	0.46
1.293	4	-3.870	0.10	0.01	1.57
	8	-3.871	0.09	0.00	0.41
1.518	4	-10.673	0.05	0.07	1.72
	8	-10.674	0.04	0.04	0.41

[1]All values are identical for models 2 and 3.

[2]As compared to elliptic integral solutions.

The potential energy of the eight element mesh is less than that of the four element mesh throughout the entire loading range. This suggests that refinements in the finite element approximation result in monotonic convergence of potential energy to that of the corresponding continuum model. No general statement can be made regarding the response predictions evaluated at given points in the assemblages. However, the eight element mesh predicts more accurate strains and displacements than the four element mesh considering the equilibrium paths in their entirety.

The relative computational efficiencies of models 2 and 3 are shown in Table 7. Model 2 is much more efficient than model 3 for an identical level of accuracy of response predictions. This is true for the four and eight element assemblages. Also, as the number of system degrees of freedom increase, the computational efficiencies of both models decrease as expected.

Inelastic Beam-Column

This test problem is investigated to compare the inelastic geometrically nonlinear response predictions of models 2 and 3.

The problem consists of a simply-supported beam-column with a constant concentric axial load. A variable transverse point load is applied at the midspan. The applied axial load is approximately 60% of the Euler buckling load. The transverse point load is incremented from zero until the limit load is attained. The material behavior is elastic-ideally plastic. The problem is defined in Figure 6.

TABLE 7. RELATIVE COMPUTATIONAL EFFICIENCIES - ELASTICA PROBLEM

Model and No. of Elements	Avg. no. of Mins. Per Load Increment[1]	Avg. Solution Time[2] Per Load Increment
Model 2 4 Elements	71.0	21.0
Model 3 4 Elements	130.2	53.4
Model 2 8 Elements	101.5	94.0
Model 3 8 Elements	174.3	185.6

[1] Magnitudes of load increments were not constant; however, identical increments were used during analysis for both models and element meshes.

[2] Seconds.

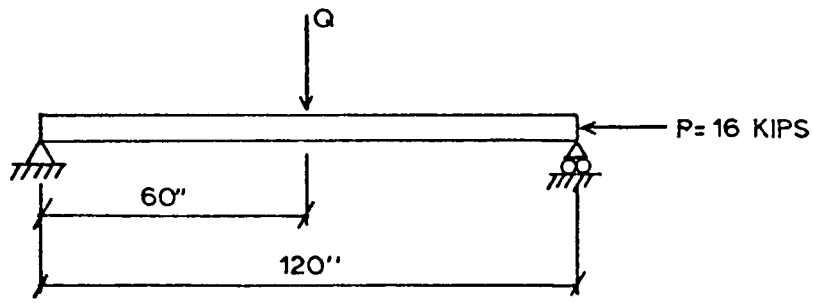

a. Longitudinal Section

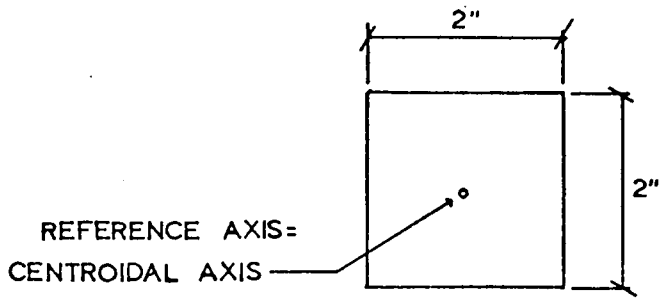

b. Cross Section

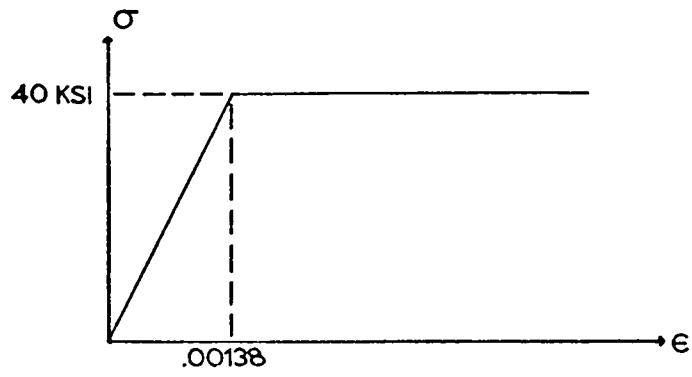

c. Constitutive Relation

FIG. 6 INELASTIC BEAM-COLUMN-TEST DESCRIPTION

The basis of comparison used in this test problem is the continuum solution obtained from the Lehigh program developed to analyze elastic-plastic beam-columns loaded at midspan by a variable transverse concentrated load [21]. The procedure used is as follows: analytical expressions relating moment, curvature, and trust are established for the different possible locations of the elastic-plastic boundaries in the beam-column. Using the central curvature of the beam-column as the dependent variable, the expressions are solved numerically for a given cross-section and axial load. The central transverse deflection as well as the end rotation of the beam-column are determined for various magnitudes of the transverse load.

The measure of micro response error selected in this test is the percent error in the approximate value of the extreme fiber compressive strain as compared to the corresponding "exact" strain value obtained by an analytical solution. The formula for the micro response error, e_m, is identical to that used in the single element test, given by Equation 9. The procedure used to calculate the "exact" extreme fiber compressive strain values at the midspan of the beam-column is as follows: using the central transverse deflections obtained from the Lehigh program, the stress resultants at the midspan of the beam-column are calculated. The strain state at the midspan can be determined from the stress resultants by conditions of equilibrium.

The test is conducted with models 2 and 3, using two, four and eight element assemblages. A seven by seven Gauss rule is used. (A similar analysis with model 1 is presented in Ref. 12).

If the load increments in the vicinity of the limit load are too large, the solution process will fail to converge to a stable equilibrium state. Therefore, small load increments must be used in the proximity of the limit load. Load increments of approximately 0.05% of the limit load predicted by the Lehigh program are used in this range. The analysis is terminated when convergence of the solution process cannot be obtained with this magnitude of load increment.

Models 2 and 3 achieve identical macro and micro response predictions in the linearly elastic range. The approximate central transverse deflection and end rotation predictions of both models converge monotonically to the exact solution as the meshes are refined. This is true throughout the linearly elastic range of response.

After initial yielding occurs in the beam-column, the response predictions of model 2 differ from the response predictions of model 3.

The inelastic range of the central transverse deflection equilibrium paths for the eight element assemblages of models 2 and 3 are shown in Figures 7 and 8, respectively. The differences in these macro response predictions of the models are very small. (The greatest difference in the predicted displacements of the models at any equilibrium state is less than 0.5%).

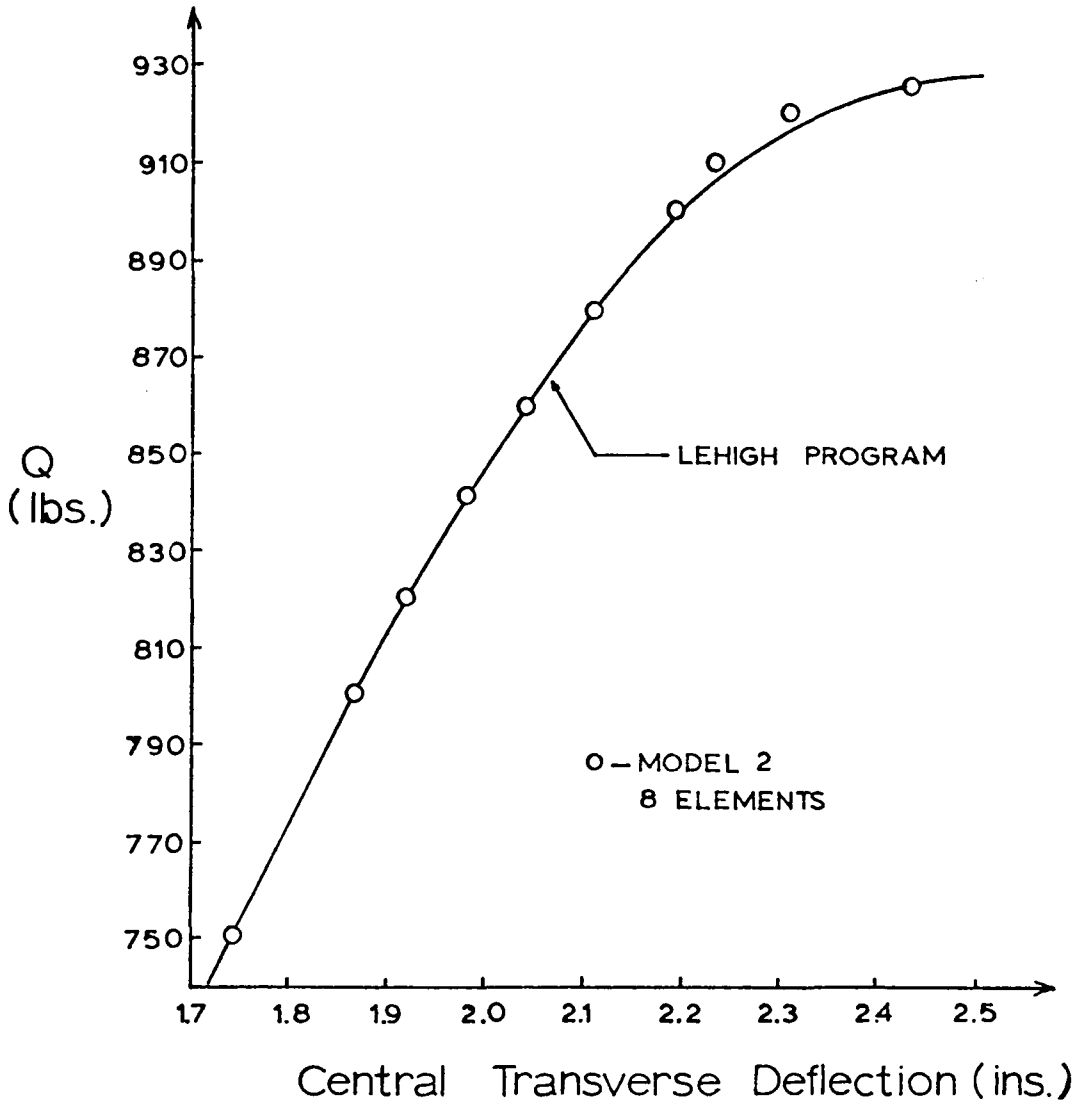

FIG. 7 CENTRAL TRANSVERSE DEFLECTION OF INELASTIC BEAM-COLUMN MODEL 2, 8 ELEMENT MESH

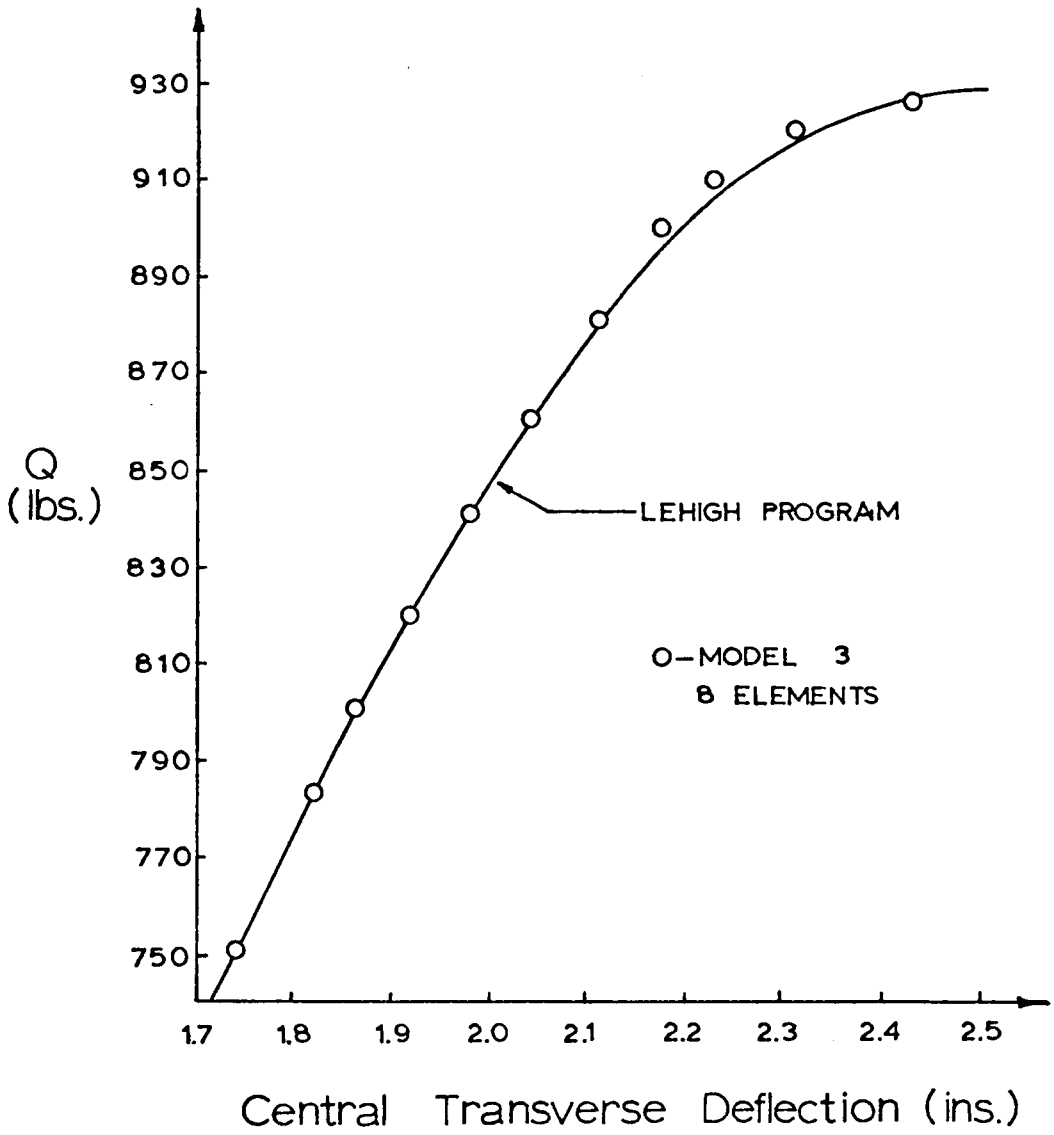

FIG. 8 CENTRAL TRANSVERSE DEFLECTION OF INELASTIC BEAM-COLUMN - MODEL 3, 8 ELEMENT MESH

The differences in the macro response predictions of the models become greater as the number of elements in the assemblages is reduced. These differences are large enough to be shown graphically in the vicinity of the limit load. In Figure 9, the central transverse deflections predicted by the two and four element meshes are shown for each model. The region shown is the vicinity of the limit point predicted by the Lehigh program in the transverse load-central transverse deflection plane.

The location of the limit point is most accurately predicted by the eight element meshes as shown in Figure 9. The limit points predicted with the two and four element meshes are represented by the last point on the respective equilibrium paths shown in the figure. The limit points predicted by both models approach the corresponding prediction of the Lehigh program as the meshes are refined.

The percent error in the central transverse deflections predicted by models 2 and 3 in the inelastic range as compared to the Lehigh program are shown in Table 8. The values are tabulated for the two, four and eight element assemblages of both models at increasing magnitudes of the transverse load. In general, both elements predict more accurate displacements as the finite element approximations are refined. At a given magnitude of the transverse load, however, mesh refinement does not guarantee more accurate macro response predictions.

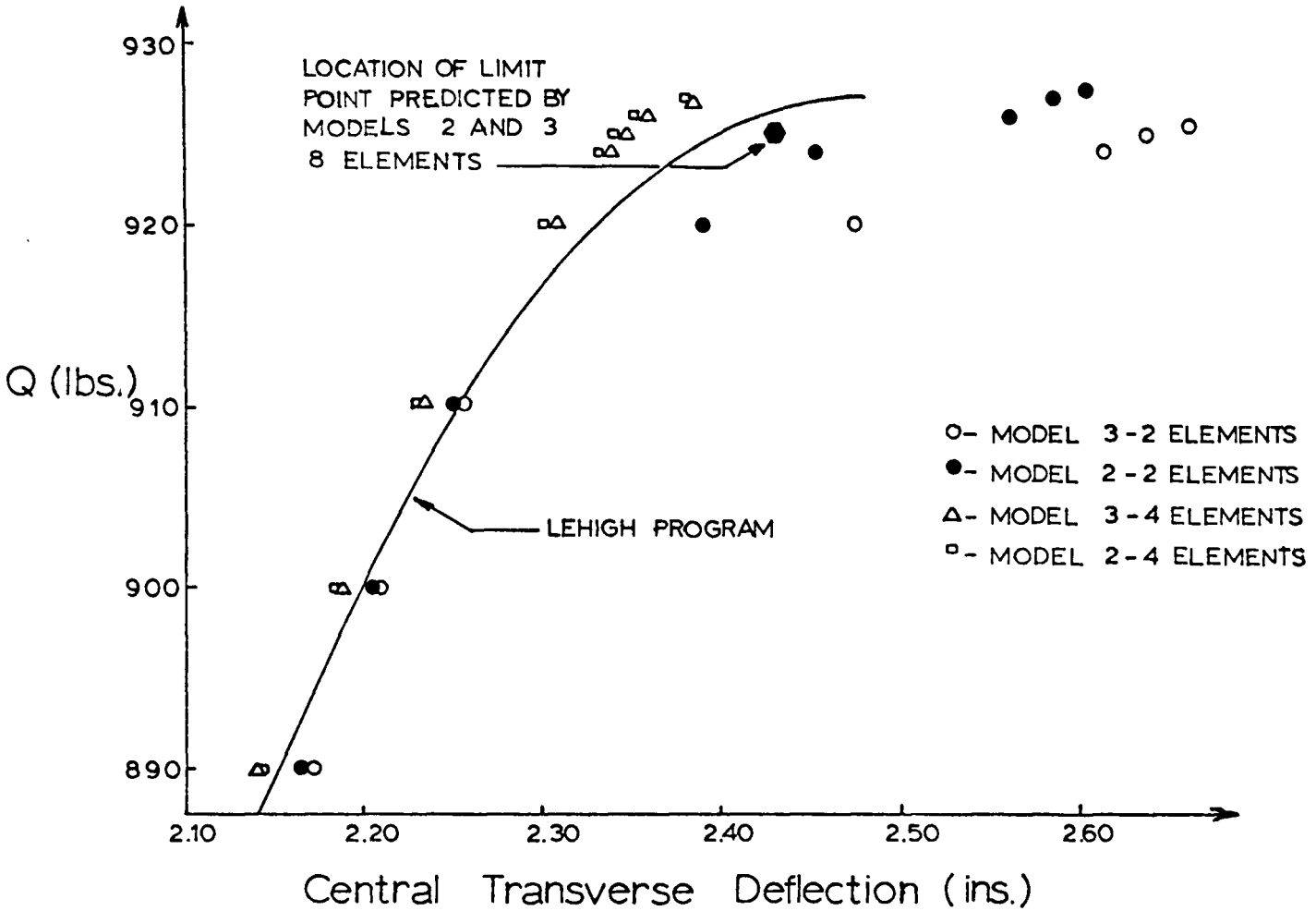

FIG. 9 CENTRAL TRANSVERSE DEFLECTION — MODELS 2 AND 3 — 2 AND 4 ELEMENTS

TABLE 8. INELASTIC MACRO RESPONSE ERROR[1] - INELASTIC BEAM-COLUMN

Q(lbs)	Model	% Error-Central Transverse Deflection		
		Number of Elements		
		2	4	8
750	2	0.34	0.21	0.20
	3	0.28	0.21	0.20
800	2	0.27	0.26	0.17
	3	0.31	0.28	0.20
840	2	0.53	0.27	0.19
	3	0.60	0.28	0.19
880	2	0.62	0.33	0.25
	3	0.83	0.36	0.25
920	2	2.26	1.12	0.86
	3	6.20	0.96	0.75

[1]As compared to Lehigh program.

No general statement can be made concerning the relative predictive accuracies of the models. Model 2 tends to predict the transverse deflection more accurately than model 3 with the two and eight element assemblages, if the entire inelastic equilibrium path is considered. The only case where model 3 achieves consistently more accurate macro response predictions than model 2 is in the vicinity of the limit point with the four element assemblages (see Figure 9). As a rule, the differences in the macro response predictions of the models are small (see Table 8). Also, both models have similar macro response convergence characteristics.

The micro response error, e_m, of the models in the inelastic range is shown in Table 9 for the two, four, and eight element assemblages. Over the entire inelastic range, mesh refinement tends to result in more accurate micro response predictions for both models. Model 2 is seen to give more accurate strain predictions than model 3 for each mesh until the limit load is approached. In the vicinity of the limit load, model 3 performs better than model 2 with respect to micro response predictions obtained with the four and eight element meshes.

The relative computational efficiencies of the models are presented in Table 10. The computational efficiency of each model decreases as the number of system generalized coordinates is increased. As in the previous test problems, model 2 is much more efficient than model 3 for each assemblage.

TABLE 9. INELASTIC MICRO RESPONSE ERROR - INELASTIC BEAM-COLUMN

Q(lbs)	Model	e_m(%) Number of Elements		
		2	4	8
750	2	7.60	2.40	0.66
	3	7.70	2.42	0.54
800	2	7.06	2.17	0.72
	3	7.53	2.40	0.89
840	2	6.52	1.70	0.83
	3	7.01	2.07	0.91
880	2	4.88	0.02	0.72
	3	5.73	0.37	0.72
920	2	2.84	2.86	1.38
	3	8.37	2.00	0.88

TABLE 10. RELATIVE COMPUTATIONAL EFFICIENCIES[1] - INELASTIC BEAM-COLUMN

Number of Elements	Model	Avg. No. of Mins. Per Load Increment	Avg. Solution Time Per Load Increment[2]
2	2	23.4	21.3
	3	42.0	46.3
4	2	38.8	79.3
	3	82.5	171.0
8	2	89.8	400.1
	3	160.8	903.5

[1] All values are based on the loading range from Q = 750 to 920 pounds. The load increments in this range are identical for all cases.

[2] Seconds.

Inelastic Restrained Beam

The purpose of this test problem is to compare the inelastic geometrically nonlinear response predictions of the models.

The problem consists of a simply-supported restrained beam subjected to a uniform transverse distributed load. The material behavior is elastic-ideally plastic. A description of the problem is presented in Figure 10.

The basis of comparison used in this test problem is the finite element solution obtained by Armen, et al. [11]. This solution is formulated within the framework of the direct stiffness method. Geometric nonlinearities are accounted for by the implementation of an incremental stiffness matrix. An initial strain vector represents the effects of plastic strains.

The finite element solution for models 2 and 3 is conducted with a six element idealization for the half-length of the beam. A seven by seven Gauss rule is used. The central transverse deflection values obtained from the solutions are compared to the values obtained from the incremental stiffness solution. (A continuum solution for this problem is not available.)

The results of the test are presented in Figure 11. The dotted line in the figure corresponds to the linearly elastic soltuion of the problem found in Ref. 11.

In the linearly elastic range of response, the models predict identical responses.

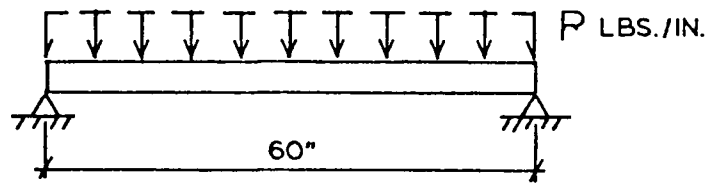

a. Longitudinal Section

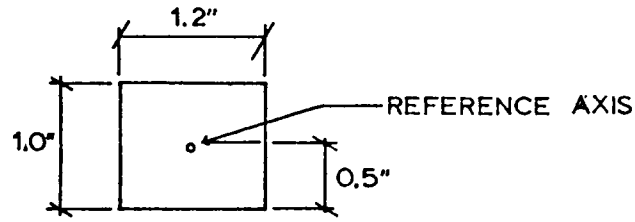

b. Cross Section

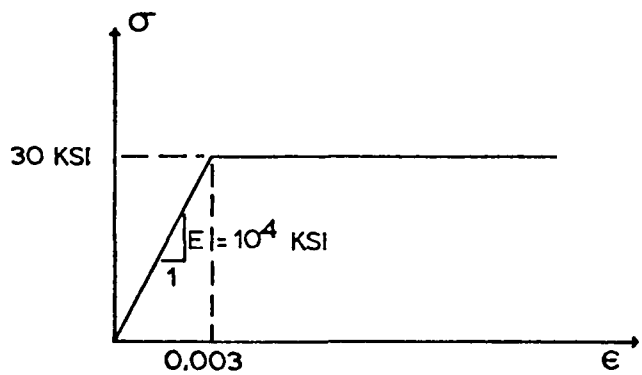

c. Constitutive Law

FIG. 10 INELASTIC RESTRAINED BEAM – TEST DESCRIPTION

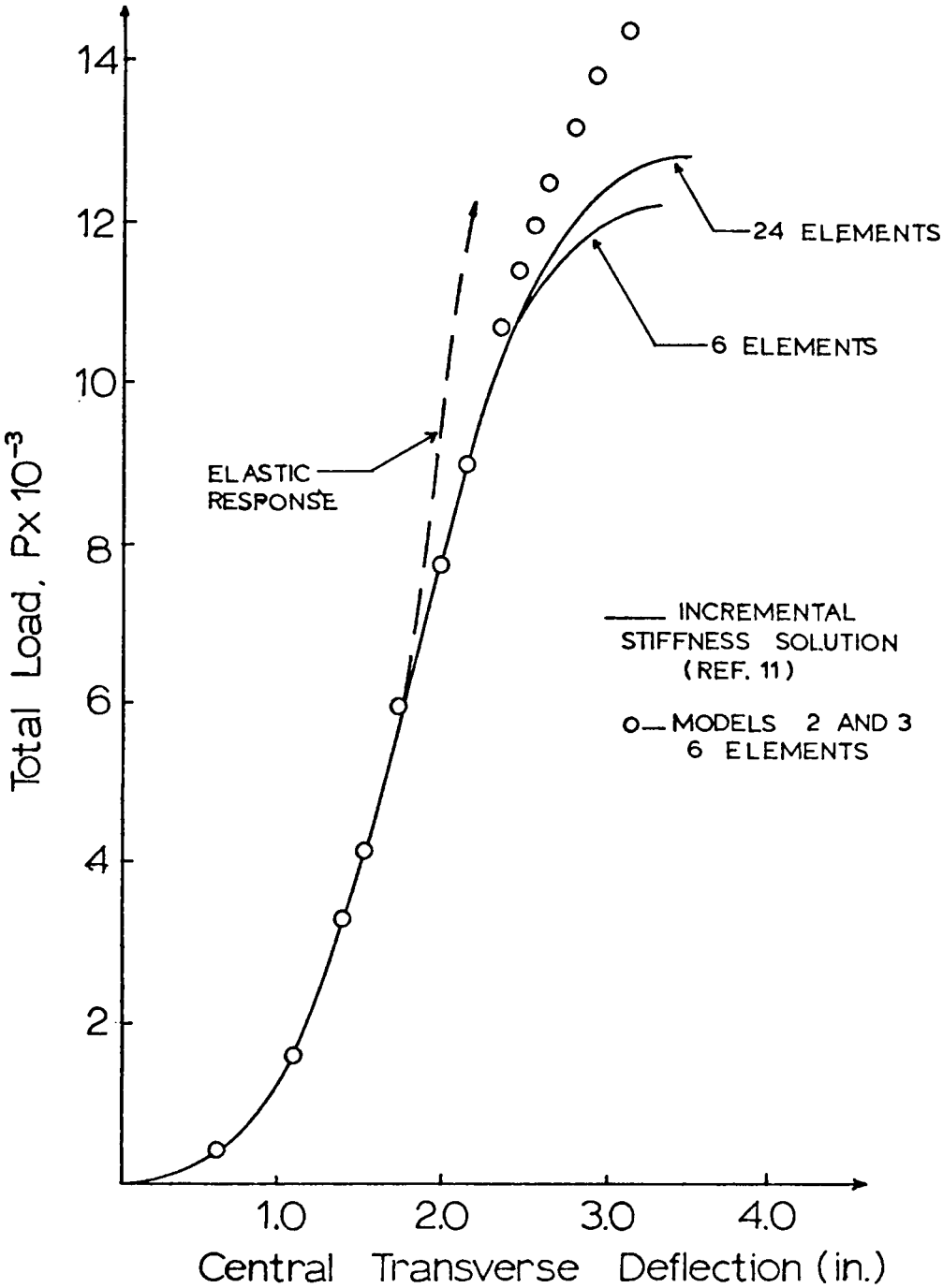

FIG. 11 CENTRAL TRANSVERSE DEFLECTION—INELASTIC RESTRAINED BEAM

After initial yielding occurs in the beam, the response predictions of model 3 differ from those of model 2. The differences in the predicted deflections of the models are small. (Considering the entire inelastic equilibrium paths, the greatest difference in these predictions is less than 0.3%.) Also, the predicted deflections of model 2 tend more closely to the corresponding stiffness solution values. The central transverse deflection predictions of each model are represented by the same points in Figure 11.

The correlation between the stiffness solution and the predictions of models 2 and 3 is favorable for the majority of the equilibrium path. The solutions diverge only after the ends of the beam become fully plastic. After this occurs, the predictions of model 2 and 3 indicate stiffness in the beam is still present. The incremental solution predicts collapse soon after the ends of the beam become fully plastic. Observe that part of the equilibrium paths predicted by models 2 and 3 and the incremental stiffness solution are nearly linear even though yielding in the beam has occurred. This is because of the counterbalancing effect of material and geometric nonlinearities on the stiffness of the beam [11].

The relative computation efficiencies of the models are shown in Table 11. Model 2 is seen to be much more computationally efficient than model 3 in this test problem.

TABLE 11. RELATIVE COMPUTATIONAL EFFICIENCIES - INELASTIC RESTRAINED BEAM

	Avg. No. of Mins. Per Load Increment	Avg. Solution Time Per Load Increment[1]
Model 2	53.0	143.6
Model 3	88.3	279.0

[1]Seconds.

CHAPTER IV

EVALUATION OF MODELS

An evaluation of models 2 and 3, based on the results of the test problems shown in Chapter III, is presented in this chapter. The evaluation is divided into two categories:

1. Evaluation of linearly elastic response predictions.
2. Evaluation of inelastic response predictions.

A commentary on the models' computational efficiencies is presented in the last section of this chapter.

Linearly Elastic Response Evaluation

In all test problems, models 2 and 3 exhibit identical response predictions in the linearly elastic range. This can be explained by examining the contributions of the internal axial deformation components to the element energy functions and gradients of both models.

The gradients of the energy function of each model are equated to zero at a stable equilibrium state. The conditions of equilibrium are:

$$G_i = \frac{\partial \pi}{\partial qi} - Q_i = 0 \qquad i = 1, 2, \ldots, NDF \qquad (10)$$

where

NDF = number of degrees of freedom of the assemblage

Q_i = i^{th} external generalized force component

q_i = i^{th} generalized coordinate

π = internal energy of the system

G_i = i^{th} gradient of the energy function

The internal energy of the system is the sum of the element internal energies, so that

$$\pi = \sum_{m=1}^{nm} \pi_m \tag{11}$$

where

π_m = internal energy of m^{th} element

nm = total number of elements in the system

Therefore

$$\frac{\partial \pi}{\partial q_i} = \sum_{m=1}^{nm} \frac{\partial \Pi_m}{\partial q_i} \tag{12}$$

If the system is linearly elastic, then

$$\Pi_m = \frac{E}{2} \iiint_V \varepsilon^2(x,y)\, dv \tag{13}$$

where V is the volume of element m, E is the modulus of elasticity of the linearly elastic constitutive law, $\varepsilon(x,y)$ is the strain field of the element and x and y are the longitudinal and transverse coordinates, respectively.

For model 2, the element deformation vector is comprised of $\bar{u}_1$, $\bar{u}_2$, $\bar{u}_3$, and $\bar{u}_4$ (see Figure 1b for a description of the element deformation vector corresponding to model 2). Therefore,

$$\pi_m = \pi_m(\bar{u}_1, \bar{u}_2, \bar{u}_3, \bar{u}_4)$$

Application of the chain rule for partial differentiation to π_m yields

$$\frac{\partial \pi_m}{\partial q_i} = \sum_{k=1}^{4} \frac{\partial \pi_m}{\partial \bar{u}_k} \frac{\partial \bar{u}_k}{\partial q_i} \tag{14}$$

where k defines the element deformation components of member m.

If ℓ is equal to the number of joint degrees of freedom in the system, then

$$j = \ell + m \tag{15}$$

Since the internal deformation components are generalized coordinate,

$$q_j = \bar{u}_{4m} \tag{16}$$

for $m = 1, \ldots, nm$

where

$\bar{u}_{4m}$ = internal axial deformation component of element m

External generalized forces are applied only at the joints, so that

$$Q_j = 0 \qquad m = 1, \ldots, nm \tag{17}$$

where j is defined by Equation 15. Using Equations 10 and 17, the conditions of internal equilibrium are

$$\frac{\partial \pi}{\partial q_j} = \frac{\partial \pi}{\partial u_{4m}} = 0 \qquad m = 1, \ldots, nm \tag{18}$$

where j is defined by Equation 15. Because $\bar{u}_{4m}$ is defined as a generalized coordinate of the system,

$$\frac{\partial \bar{u}_{km}}{\partial \bar{u}_{4m}} = \begin{matrix}(0 \text{ if } k \neq 4) \\ (1 \text{ if } k = 4)\end{matrix} \qquad m = 1, \ldots, nm \tag{19}$$

so that

$$\frac{\partial \pi_a}{\partial \bar{u}_{4m}} = 0 \text{ if } a \neq m, \qquad \begin{matrix}a = 1, \ldots, nm \\ m = 1, \ldots, nm\end{matrix} \tag{20}$$

Using Equations 12, 14, 18, 19, and 20, conditions of element internal compatibility are

$$\frac{\partial \pi_m}{\partial \bar{u}_{4m}} = 0 \qquad m = 1, \ldots, nm \tag{21}$$

If the reference axis and centroidal axis of element m coincide, integration of the element internal-energy density over the volume of the element m by Equation 13 and application of Equation 21 yield

$$\bar{u}_4 = \frac{L}{64} (\bar{u}_3^2 - \bar{u}_2^2) \tag{22}$$

where L is the element length and $\bar{u}_2$, $\bar{u}_3$, and $\bar{u}_4$ are element deformation components of element m. This is true for each element if the material behavior of the element is linearly elastic and the element's centroidal axis and reference axis coincide.

For model 3,

$$\pi_m = \pi_m (\bar{u}_1, \bar{u}_2, \bar{u}_3, \bar{u}_4, \bar{u}_5)$$

where $\bar{u}_1$, $\bar{u}_2$, $\bar{u}_3$, $\bar{u}_4$ and $\bar{u}_5$ are the element deformation components corresponding to model 3 (see Figure 1c for a description of these components).

A similar procedure to that used for model 2 can be employed to express $\bar{u}_4$ and $\bar{u}_5$, the internal deformation components of model 3, in terms of $\bar{u}_1$, $\bar{u}_2$, and $\bar{u}_3$ for element m as

$$\bar{u}_4 = \frac{-1}{3}\bar{u}_1 + \frac{L}{54}(\bar{u}_3^2 - \bar{u}_2^2) - \frac{L}{162}(\bar{u}_2 - \bar{u}_3)^2 \qquad (23)$$

and

$$\bar{u}_5 = \frac{1}{3}\bar{u}_1 + \frac{L}{54}(\bar{u}_3^2 - \bar{u}_2^2) + \frac{L}{162}(\bar{u}_2 - \bar{u}_3)^2 \qquad (24)$$

where L is the length of element m.

As with model 2, this is true only if the material behavior is linearly elastic and the element's centroidal axis and reference axis coincide. Using Equations 13, 22, 23, and 24, the respective element internal energy expressions for each model can be shown to be identical functions of $\bar{u}_1$, $\bar{u}_2$, and $\bar{u}_3$. Since $\bar{u}_1$, $\bar{u}_2$, and $\bar{u}_3$ are identical functions of the joint generalized coordinates for both models, Equation 10 is also identical for both models. This guarantees identical macro response predictions for the two models in the linearly elastic range of response.

By substituting Equation 22 into the strain-displacement relation of model 2 and substituting Equations 23 and 24 into the strain-displacement relation of model 3, equivalent strain-displacement relations are obtained for both models in terms of $\bar{u}_1$, $\bar{u}_2$, and $\bar{u}_3$. $\bar{u}_1$, $\bar{u}_2$, and $\bar{u}_3$ are defined identically in terms of the joint generalized coordinates for both models. Therefore, this explains the equality of micro response predictions of the models in the linearly elastic range of response as shown in Chapter III.

The strain-displacement relations of both models can be expressed as

$$\varepsilon(t,s) = \frac{2}{L}\bar{u}_1 + \frac{1}{15}\left(\bar{u}_2^2 - \frac{1}{2}\bar{u}_2\bar{u}_3 + \bar{u}_3^2\right) - s[(3t - 1)\bar{u}_2 + (3t + 1)\bar{u}_3] \tag{25}$$

where s, t, $\bar{u}_1$, $\bar{u}_2$, $\bar{u}_3$ and L are as defined in Figures 1b and c. This is true only if the material behavior is linearly elastic and the element's reference axis and centroidal axis are coincidental.

Examination of Equation 25 shows that the extensional strain is represented by a constant in terms of $\bar{u}_1$, $\bar{u}_2$ and $\bar{u}_3$.

A variational formulation of the classical beam-column problem yields the differential equation of axial equilibrium [9,13].

$$EA\frac{d}{dx}\left[\frac{du}{dx} + \frac{1}{2}\left(\frac{dv}{dx}\right)^2\right] = 0 \tag{26}$$

In Equation 26, u is the axial displacement, v is transverse displacement, x is the longitudinal coordinate, A is the cross-sectional area of the beam-column, and E is the modulus of elasticity. Equation 26 implies that the extensional strain is constant along the length of the beam-column. This is analogous to the constant extensional strain state predicted by Equation 25 for element models 2 and 3.

If the reference axis and the centroidal axis of an element do not coincide, Equation 25 is not true. In this case, the original extensional strain functions of both models apply (see Equations 9 and 10). The extensional strain functions of the models can admit the same polynomial variation as the bending strain in the longitudinal direction of an element. It has been shown that this is a necessary condition for the independence of the strain state of an element and the location of the reference axis in the plane of the element [14]. (This condition is required for accurate modeling of plane frames in which members of different cross-sectional areas intersect [2].)

The linearly elastic response predictions of the models as observed in Chapter III are excellent. As shown in the single element test, the models can represent a simple bending state exactly. The elastica problem demonstrates the models' capabilities to predict large displacements and rotations (large geometric nonlinearities) with a high degree of accuracy. Mesh refinement does not guarantee uniform convergence of strains and displacements in this range. However, mesh refinement is seen to increase each model's accuracy of

macro and micro response predictions considering the entire equilibrium paths.

The poor computational efficiency of model 3, as compared to model 2, eliminates any possible applications of the model in the linearly elastic range of response. Since both models achieve identical response predictions in this range, the more efficient model, model 2, should be used in any linearly elastic analysis.

Inelastic Response Evaluation

The inelastic response predictions of model 2 differ from those of model 3 in the last two test problems of Chapter III. This is not true for all cases of inelastic responses predicted by the models. As shown in the single element test, if physical nonlinearities and no geometric nonlinearities occur, both models exhibit identical response predictions.

A necessary condition for the response predictions of the two models to be different is that the second order longitudinal variation of the extensional strain component of model 3 not vanish. The conditions for the vanishing of this term are defined by Equations 23 and 24, derived in the preceding section of this chapter. These equations are derived by assuming linearly elastic material behavior. No such expressions can be written if the constitutive law is not a continuous linear function. More generally, if the material response is nonlinear and geometric nonlinearities are present, the responses predicted by model 2 will differ from the response predictions of

model 3. If both types of nonlinearity are present in an element, the extensional strain component of model 2 will vary linearly along the length of the element. The extensional strain predicted by model 3 will then vary quadratically along the length of an element. This is as observed in the test problems.

The results of the test problems indicate that the response predictions of the models in the inelastic range are excellent. Also, mesh refinement results in increased accuracy of the responses predicted by the models.

The computational efficiency of model 2 is clearly superior to that of model 3 in the inelastic range. However, the test results are inconclusive as to the relative predictive merits of the models.

In all cases, the differences in the responses predicted by each model are small. As the meshes are refined, these differences become smaller. Considering the test problems examined, no consistent gains in predictive accuracy are realized with model 3 as compared to model 2.

As a rule, the responses predicted by model 2 tend to be more accurate than the response predictions of model 3, considering the entire equilibrium paths predicted by the models. Hodge states that increased element complexity in plastic analysis may not increase the accuracy of response predictions [8]. This statement seems to be true in regard to the models investigated in this study.

Further testing of the models in the inelastic range could conceivably yield situations where model 3 consistently predicts

more accurate responses than model 2. However, from the results of this study, this seems unlikely. On the basis of this investigation model 2 is seen to be the superior element model for inelastic analysis.

Comments on Computational Efficiency

Throughout the entire range of response, including the linearly elastic and inelastic ranges, model 2 is considerably more computationally efficient than model 3. This fact is evidenced by examining the relative computational efficiency information presented in Chapter III.

Model 3 has eight element degrees of freedom. Model 2 has seven element degrees of freedom. Therefore, for a given assemblage of n elements, the assemblage modeled with elements corresponding to model 3 will contain n more generalized coordinates than the assemblage comprised of model 2 elements. The computational efficiency data presented in Chapter III indicates that the numeric increase of generalized coordinates produced by model 3 cannot fully explain the model's poor relative computational efficiency. This suggests that the two internal axial deformation components of model 3 produce a deleterious effect on the sensitivity of the corresponding energy function.

As stated in Chapter II, the computation required to establish a stable equilibrium state with the minimization process used in this study is dependent on the sensitivity of the energy function

to changes in each of the generalized coordinates [16]. If the energy function is disproportionately sensitive to changes in certain generalized coordinates, the energy function is considered to be geometrically eccentric [16].

The "ideal" condition for optimization by gradient techniques occurs when the objective function is geometrically concentric, i.e. the objective function represents a family of hyperspheroids in n-dimensional space, where n is the number of independent variables [16].

In general, this ideal situation can rarely be realized. In order to decrease the geometric eccentricity of an objective function, scaling of the independent variables is frequently employed [16].

Gottfried and Weisman suggest the following procedure for scaling independent variables (generalized coordinates): the variables are scaled in such a fashion that a unit change in any one of the scaled variables at the optimum (minimum) will effect the objective function (energy function) to the same extent as a unit change in any of the other scaled variables at the optimum [16]. In effect, this procedure decreases the geometric eccentricity of the objective function at the optimum.

A simple numerical experiment is performed to qualitatively assess the geometric eccentricity of the energy functions of both models at a stable equilibrium state. The procedure used is analogous to the scaling procedure described above. It should be noted that the experiment has no real physical significance and is limited in its

scope of application. However, it does illustrate qualitatively some characteristics observed in the test problems.

The procedure used is as follows: a single element in the unstrained state (the energy function is a minimum at this state) is subjected to individual unit changes in some of its generalized coordinates. The changes correspond to a unit axial displacement at one end of the element, a unit end rotation, and a unit change in the respective internal axial deformation components. The test is performed on both models for varying aspect ratios. Linearly elastic material response is assumed. The depth of the element's cross-section, the cross-sectional area and the modulus of elasticity are unity. The changes in the models' internal energies associated with each corresponding unit change in the respective generalized coordinates are observed.

The results of the experiment are presented in Figure 12. L/h is the element's aspect ratio and $\frac{\Delta\Pi}{AEL}$ represents the nondimensionalized change in energy. Each curve represents a unit change in one of the generalized coordinates of the model. A geometrically concentric energy function would be represented by a single curve, i.e. the curves representing a unit change in each of the generalized coordinates would be coincidental. Observe that the changes in energy associated with the internal axial deformation components become much greater than the changes associated with the remaining generalized coordinates as the aspect ratio decreases. For increasing aspect ratios greater than

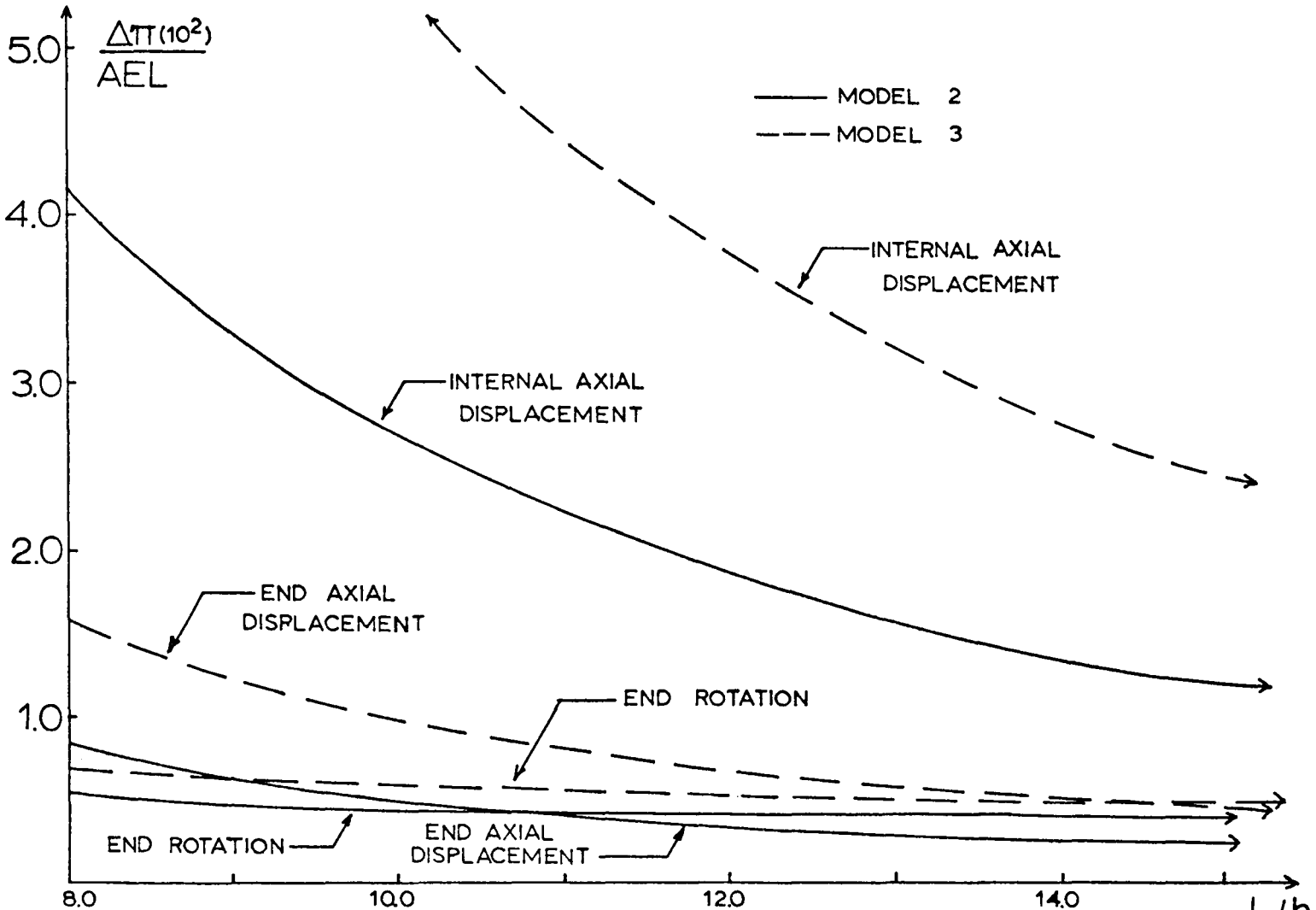

FIG. 12 CHANGES IN ENERGY FOR UNIT CHANGES IN GENERALIZED COORDINATES

15, the dominant changes in energy are caused by the unit rotations for both models.

In the single element test, the number of minimizations required to establish an equilibrium path for model 3 increases as the aspect ratio decreases. This is consistent with the predicted variation of the geometric eccentricity of the energy function as the aspect ratio is decreased for model 3 (see Figure 12).

For model 2, the fewest number of minimizations required to establish an equilibrium path in the single element test occurs when $L/h = 15$. The results shown in Figure 12 imply that the geometric eccentricity of the energy function of model 2 is small for this aspect ratio.

The results of this experiment imply that the geometric eccentricity of the energy function of model 3 is greater than that of model 2. (This implication is for the aspect ratios used in the test problems examined in this study.) This is a plausible explanation for the poor relative computational efficiency of model 3 observed in the test problems.

Fox and Stanton have found scaling procedures to be effective for structural analysis by energy minimization. Also, these procedures were found to be beneficial in conjunction with the variable-metric gradient algorithm (the minimization procedure used in this study) [10].

Further tests, similar to the one conducted here, could yield scaling factors for the generalized coordinates of both models.

This could enhance the computational efficiencies of the models considerably.

CHAPTER V

CONCLUSION

The comparison and convergence studies conducted in this investigation indicate that models 2 and 3 predict accurate responses throughout the entire range of response. Mesh refinement in both the linearly elastic and inelastic ranges enhances the accuracy of the models' response predictions.

In the linearly elastic range, the models predict identical responses.

The response predictions of model 2 are not identical to the response predictions of model 3 in the inelastic range. The differences in these response predictions are small. As a rule, greater predictive accuracy is achieved with model 2.

The computational efficiency of model 2 is much greater than that of model 3 throughout the range of response.

On the basis of the tests conducted in this study, the efficiency of response of model 2 is seen to be clearly superior to that of model 3 throughout the entire range of response. However, the inelastic test results are inconclusive. It is conceivable that under some circumstances in the inelastic range, model 3 could predict more accurate responses than model 2. This seems unlikely, however, considering the relative performances of the models in the inelastic range in this investigation.

Refinements could possibly be made to model 2 to enhance its computational efficiency. For linearly elastic analyses, condensation of the internal axial deformation component could be implemented. This would reduce the number of system generalized coordinates resulting in increased computational efficiency. Also, parametric studies could be conducted to develop a procedure to scale the generalized coordinates. This could possibly yield significant increases in the computational efficiency of the model.

REFERENCES

1. Holzer, S. M., Melosh, R. J., Barker, R. M., and Somers, A. E., "SINGER: A Computer Code for General Analysis of Two-Dimensional Concrete Structures," Technical Report No. AFWL-TR-74-228, Vol. 1, Air Force Weapons Laboratory, Kirtland Air Force Base, N.M., May 1975.

2. Bradshaw, J. C., "Nonlinear Analysis of Plane Frames," Master Thesis, Virginia Polytechnic Institute and State Univ., Blacksburg, Va., May 1975.

3. Timoshenko, S. P., and Gere, J. M., Theory of Elastic Stability, McGraw-Hill, N.Y., 1961.

4. Holzer, S. M., Somers, A. E., and Bradshaw, J. C., "Reliability Study of SINGER," Technical Report No. AFWL-TR-76-192, Vol. 1, Air Force Weapons Laboratory, Kirtland Air Force Base, N.M., 1976.

5. Zienkiewicz, O. C., The Finite Element Method in Engineering Science, McGraw-Hill, London, 1971.

6. Gallagher, R. H., Finite Element Analysis Fundamentals, Prentice-Hall, Inc., Englewood Cliffs, N.J., 1975.

7. Langhaar, H. L., Energy Methods in Applied Mechanics, John Wiley and Sons, Inc., N.Y., 1962.

8. Hodge, P. G., "Computer Solutions of Plasticity Problems," Report H1-3, Department of Aerospace Engineering and Mechanics, Univ. of Minnesota, Minneapolis, Minn., Sept., 1972.

9. Dym, C. L., and Shames, I. H., Solid Mechanics: A Variational Approach, McGraw-Hill, Inc., N.Y., 1973.

10. Fox, R. L., and Stanton, E. L., "Developments in Structural Analysis by Direct Energy Minimization," Journal of the American Institute of Aeronautics and Astronautics, Vol. 6, No. 6, June 1968, pp. 1036-1042.

11. Armen, H., Pifko A., and Levine, H. S., "A Finite Element Method for the Plastic Bending Analysis of Structures," Proceedings of the Second Air Force Conference on Matrix Methods in Structural Mechanics, Wright-Patterson Air Force Base, Ohio, 1968.

12. Shiflett, R. B., "Analysis of Nonlinear Beam-Columns," Master Thesis, Virginia Polytechnic Institute and State Univ., Blacksburg, Va., April, 1977.

13. Simitses, G. J., An Introduction to the Elastic Stability of Structures, Prentice-Hall, Inc., Englewood Cliffs, N.J., 1976.

14. Holzer, S. M., and Somers, A. E., "Nonlinear Model/Solution Process: An Energy Approach," Journal of the Engineering Mechanics Division, ASCE, August, 1977.

15. Melosh, R. J., "Manipulation Errors in Finite Element Analysis," Recent Advances in Matrix Methods of Structural Analysis and Design, (R. H. Gallagher, Y. Yamada, and J. T. Oden, Eds.), University of Alabama Press, Huntsville, Ala., 1971.

16. Gottfried, B. S., and Weisman, J., Introduction to Optimization Theory, Prentice-Hall, Inc., Englewood Cliffs, N.J., 1973.

17. Fletcher, R., and Powell, M. J. D., "A Rapidly Convergent Descent Method for Minimization," The Computer Journal, Vol. 6, No. 2, July 1963, pp. 163-170.

18. Fried, A., "Shape Functions and the Accuracy of Arch Finite Elements," Journal of the American Institute of Aeronautics and Astronautics, Vol. 11, No. 3, 1973, pp. 287-291.

19. Oliveira, E. R. A., "Mathematical Theory of Linear Structures," Lectures on Finite Element Methods in Continuum Mechanics, (J. T. Oden, E. R. A. Oliveira, Eds.), University of Alabama Press, Ala., 1973.

20. Oliveira, E. R. A., "Theoretical Foundations of the Finite Element Method," International Journal of Solids and Structures, Vol. 4, 1968, pp. 929-952.

21. Iyengar, S., and Chen, W. F., "Computer Program for an Inelastic Beam-Column Problem," Fritz Engineering Laboratory Report No. 331.7, Lehigh University, Bethleham, Pa., 1970.

APPENDIX

STRAIN FIELD DERIVATION FOR MODEL 3

STRAIN-FIELD DEVIATION FOR MODEL 3

For the transformations relating the element deformation components $\bar{u}_1$, $\bar{u}_2$, and $\bar{u}_3$ to the generalized coordinates, see Ref. 4. $\bar{u}_1$, $\bar{u}_2$, $\bar{u}_3$, $\bar{u}_4$, $\bar{u}_5$, L, X, Y, s, and t are defined in Figure 1c.

Axial Interpolation

The axial deflection u, is expressed using Lagrangian interpolation as

$$u(t) = \ell_1 u(-1) + \ell_2 u(\tfrac{-1}{3}) + \ell_3 u(\tfrac{1}{3}) + \ell_4 u(1) \tag{1}$$

where

$$\ell_1 = \frac{-9}{16}\left(t^3 - t^2 - \frac{t}{9} + \frac{1}{9}\right) \tag{2}$$

$$\ell_2 = \frac{27}{16}\left(t^3 - \frac{1}{3}t^2 - t + \frac{1}{3}\right) \tag{3}$$

$$\ell_3 = \frac{-27}{16}\left(t^3 + \frac{1}{3}t^2 - t - \frac{1}{3}\right) \tag{4}$$

$$\ell_4 = \frac{9}{16}\left(t^3 + t^2 - \frac{1}{9}t - \frac{1}{9}\right) \tag{5}$$

From Figure 1c,

$$-u(-1) = u(1) = \bar{u}_1 \tag{6}$$

$$u(-\tfrac{1}{3}) = \bar{u}_4 \tag{7}$$

$$u(\tfrac{1}{3}) = \bar{u}_5 \tag{8}$$

Substitution of Equations 6, 7, and 8 into Equation 1 yields

$$u(t) = \Phi_1 \bar{u}_1 + \Phi_4 \bar{u}_4 + \Phi_5 \bar{u}_5 \tag{9}$$

where

$$\Phi_1 = \frac{9}{8}\left(t^3 - \frac{t}{9}\right) \tag{10}$$

$$\Phi_4 = \frac{27}{16}\left(t^3 - \frac{1}{3}t^2 - t + \frac{1}{3}\right) \tag{11}$$

$$\Phi_5 = \frac{-27}{16}\left(t^3 + \frac{1}{3}t^2 - t - \frac{1}{3}\right) \tag{12}$$

Transverse Interpolation

The transverse deflection v can be expressed as

$$v(t) = \Phi_2 q_2 + \Phi_3 q_3 \tag{13}$$

where Φ_2 and Φ_3 are Hermite polynomials and

$$q_2 = \bar{u}_2 \frac{L}{2} \tag{14}$$

$$q_3 = \bar{u}_3 \frac{L}{2} \tag{15}$$

$$\Phi_2 = \frac{1}{4}(t + 1)(t - 1)^2 \tag{16}$$

$$\Phi_3 = \frac{1}{4}(t - 1)(t + 1)^2 \tag{17}$$

From the boundary conditions (see Figure 1c)

$$v(-1) = v(1) = 0 \tag{18}$$

$$\frac{dv(-1)}{dx} = \bar{u}_2 \tag{19}$$

$$\frac{dv(1)}{dx} = \bar{u}_3 \tag{20}$$

Strain Field

The strain-displacement relation of the beam-column is defined as

$$\varepsilon(x,y) = \frac{du}{dx} + \frac{1}{2}\left(\frac{dv}{dx}\right)^2 - y\frac{d^2v}{dx^2} \tag{21}$$

Equation 21 is expressed in terms of t and s as

$$\varepsilon(t,s) = \frac{2}{L}\frac{du}{dt} + \frac{2}{L^2}\left(\frac{dv}{dt}\right)^2 - \frac{4s}{L}\left(\frac{d^2v}{dt^2}\right) \tag{22}$$

The extensional strain, represented by the first two terms of Equation 22, are constrained to be quadratic in t so that

$$\varepsilon(t,0) = \frac{2}{L}\frac{du}{dt} + \frac{2}{L^2}\left(\frac{dv}{dt}\right)^2 = a_0 + a_1 t + a_2 t^2 \tag{23}$$

where a_0, a_1, and a_2 are unknown constants. The solution of Equation 23 can be expressed as

$$\frac{2}{L}\int_{-1}^{t} du = \int_{-1}^{t} (a_0 + a_1 t + a_2 t^2)\, dt - \frac{2}{L^2}\int_{-1}^{t} \left(\frac{dv}{dt}\right)^2 dt \tag{24}$$

Integrating Equation 24 and substituting the continuity conditions, Equations 6, 7, 8 yield three equations in a_0, a_1, and a_2 expressed as

$$\frac{4}{L}\bar{u}_1 = 2a_0 + \frac{2}{3}a_2 - 2c \tag{25}$$

$$\frac{2}{L}(\bar{u}_4 + \bar{u}_1) = \frac{2}{3}a_0 - \frac{4}{9}a_1 + \frac{26}{81}a_2 - 2A \tag{26}$$

$$\frac{2}{L}(\bar{u}_5 + \bar{u}_1) = \frac{4}{3}a_o - \frac{4}{9}a_1 + \frac{28}{81}a_2 - 2B \tag{27}$$

where

$$A = \frac{1}{L^2}\int_{-1}^{\frac{1}{3}} \left(\frac{dv}{dt}\right)^2 dt \tag{28}$$

$$B = \frac{1}{L^2}\int_{-1}^{\frac{1}{3}} \left(\frac{dv}{dt}\right)^2 dt \tag{29}$$

$$C = \frac{1}{L^2}\int_{-1}^{1} \left(\frac{dv}{dt}\right)^2 dt \tag{30}$$

The solution of Equations 25, 26, 27 yields

$$a_o = \frac{27}{8L}\left(\frac{-2}{27}\bar{u}_1 - \bar{u}_4 + \bar{u}_5\right) - \frac{27}{8}\left(A - B + \frac{1}{27}C\right) \tag{31}$$

$$a_1 = \frac{-9}{4L}(\bar{u}_5 + \bar{u}_4) - \frac{9}{4}(A + B - C) \tag{32}$$

$$a_2 = \frac{-81}{8L}\left(\bar{u}_5 - \bar{u}_4 - \frac{2}{3}\bar{u}_1\right) + \frac{81}{8}\left(A - B + \frac{1}{3}C\right) \tag{33}$$

From Equations 23, 31, 32, 33

$$\begin{aligned}\varepsilon(t,0) = {} & \frac{27}{8}\left[\frac{1}{L}\left(\frac{-2}{27}\bar{u}_1 - \bar{u}_4 + \bar{u}_5\right) - \left(A - B + \frac{1}{27}C\right)\right] \\ & - \frac{9}{4}\left[\frac{1}{L}(\bar{u}_5 + \bar{u}_4) + (A + B - C)\right]t + \frac{81}{8}\left[\frac{-1}{L}(\bar{u}_5 \right. \\ & \left. - \bar{u}_4 - \frac{2}{3}\bar{u}_1) + \left(A - B + \frac{1}{3}C\right)\right]t^2\end{aligned} \tag{34}$$

Substitution of Equation 9 into Equations 28, 29, 30, gives

$$A = \frac{19}{405} (\bar{u}_2^2 - \frac{1}{2} \bar{u}_2 \bar{u}_3 + \frac{4}{19} u_3^2) \tag{35}$$

$$B = \frac{1}{405} (23 \bar{u}_2^2 - 4 \bar{u}_2 \bar{u}_3 + 8 \bar{u}_3^2) \tag{36}$$

$$C = \frac{1}{15} (\bar{u}_2^2 - \frac{1}{2} \bar{u}_2 \bar{u}_3 + \bar{u}_3^2) \tag{37}$$

For simplification let

$$\alpha = \frac{-27}{8} (A - B + \frac{1}{27} C) \tag{38}$$

$$\beta = A + B - C \tag{39}$$

$$\lambda = A - B + \frac{1}{3} C \tag{40}$$

Substitution of Equations 35, 36, 37 into Equations 38, 39, 40 yields

$$\alpha = \frac{1}{40} (\bar{u}_2 + \bar{u}_3)^2 \tag{41}$$

$$\beta = \frac{1}{27} (\bar{u}_2^2 - \bar{u}_3^2) \tag{42}$$

$$\lambda = \frac{1}{81} (\bar{u}_2 - \bar{u}_3)^2 \tag{43}$$

Equation 22 can be expressed in the form

$$\varepsilon(t,s) = \varepsilon(t,0) - \frac{4s}{L} \frac{d^2v}{dt^2} \tag{44}$$

where

$$\varepsilon(t,0) = \frac{27}{8L}\left(\frac{-2}{27}\,\bar{u}_1 - \bar{u}_4 + \bar{u}_5\right) + \alpha - \frac{9}{4}\left[\frac{1}{L}\left(\bar{u}_5 + \bar{u}_4\right) + \beta\right]t + \frac{81}{8}\left[\frac{-1}{L}\left(\bar{u}_5 - \bar{u}_4 - \frac{2}{3}\,\bar{u}_1\right) + \lambda\right]t^2 \tag{45}$$

On the basis of Equations 13, 44, 45 the strain field of model 3 is defined as

$$\varepsilon(t,s) = \frac{27}{81}\left(\frac{-2}{27}\,\bar{u}_1 - \bar{u}_4 + \bar{u}_5\right) + \alpha - \frac{9}{4}\left[\frac{1}{L}\left(\bar{u}_5 + \bar{u}_4\right) + \beta\right]t + \frac{81}{8}\left[\frac{-1}{L}\left(\bar{u}_5 - \bar{u}_4 - \frac{2}{3}\,\bar{u}_1\right) + \lambda\right]t^2 - s\left[(3t - 1)\,\bar{u}_2 + (3t + 1)\,\bar{u}_3\right] \tag{46}$$

The vita has been removed from the scanned document

COMPARISON AND CONVERGENCE STUDIES OF NONLINEAR FINITE ELEMENT BEAM-COLUMN MODELS

by

George Michael Brown

(ABSTRACT)

Comparison and convergence studies are conducted with two nonlinear finite element beam-column models. Both models admit physical and geometric nonlinearities.

The models differ in their respective strain field representations. Model 2 permits a linear longitudinal and transverse strain variation. The strain field of model 3 can vary linearly in the transverse direction and quadratically in the longitudinal direction.

The system model and solution process used with both element models are identical. The system model is defined by an energy function. The equilibrium path of the system is determined at discrete load levels. At each load level, application of the solution process yields the new equilibrium configuration of the system.

Four test problems are selected to determine the relative merits of models 2 and 3. The models are tested over the entire range of response.

The tests indicate that both models predict accurate responses throughout the range of response. Mesh refinement is seen to increase the accuracy of the models' response predictions.

The models achieve identical response predictions in the linearly elastic range. The inelastic response predictions of model 2 are seen to be more accurate than those of model 3. Model 2 is computationally more efficient than model 3 over the entire range of response.

The results of the studies reveal that throughout the range of response, the efficiency of response of model 2 is greater than that of model 3.